Eberhard Karls Universität Tübingen
&
Universidad de Granada

Master Thesis

---

# Master thesis

---

*Author:*
Leopold Bodamer

*Supervisor:*
Prof. Dr. Daniel Manzano Diosdado
*Universidad de Granada*

*Examiner:*
Prof. Dr. Beatriz Olmos Sanchez
*Eberhard Karls Universität Tübingen*

*A thesis submitted in fulfillment of the requirements*
*for the degree of Master of Science*

*in*

Theoretical Atomic Physics and Synthetic Quantum Systems
Institut für Theoretische Physik

September 10, 2025

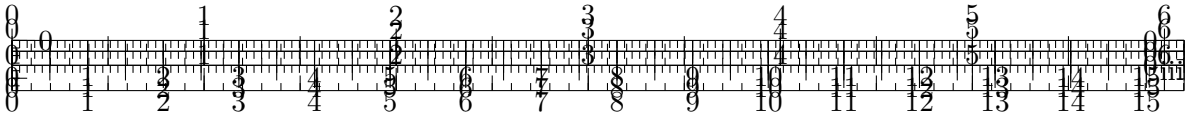

# Declaration of Authorship

I, Leopold Bodamer, declare that this thesis titled, "Master thesis" and the work presented in it are my own. I confirm that:

- This work was done wholly or mainly while applying for a research degree at this University.
- Where any part of this thesis has previously been submitted for a degree or any other qualification at this University or any other institution, this has been clearly stated.
- Where I have consulted the published work of others, this is always clearly attributed.
- Where I have quoted from the work of others, the source is always given. With the exception of such quotations, this thesis is entirely my own work.
- I have acknowledged all main sources of help.
- Where the thesis is based on work done by myself jointly with others, I have made clear exactly what was done by others and what I have contributed myself.

Signed:

Date:

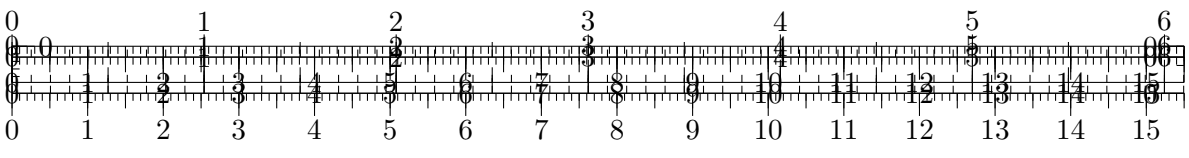

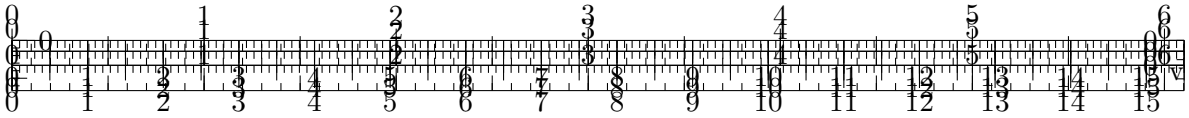

# Contents



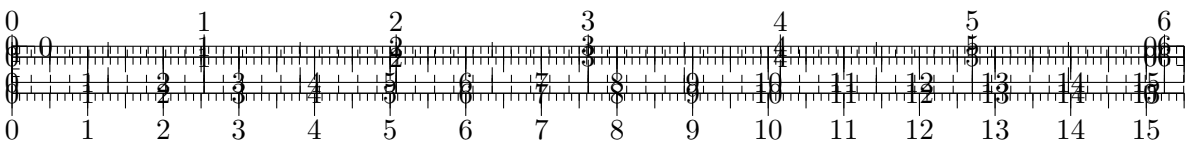

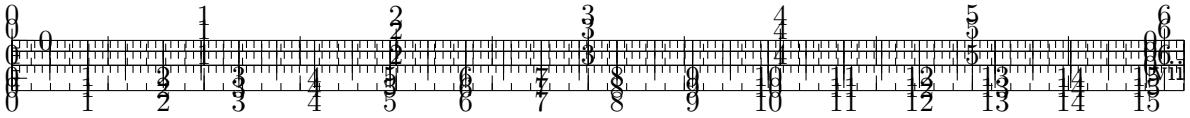



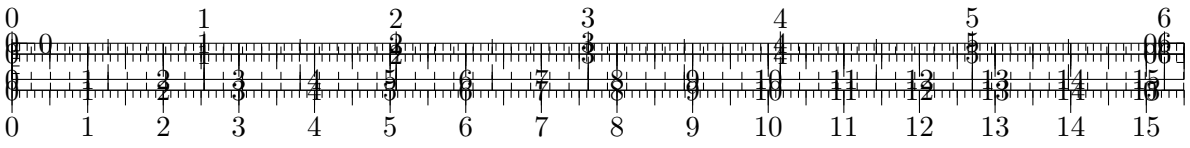

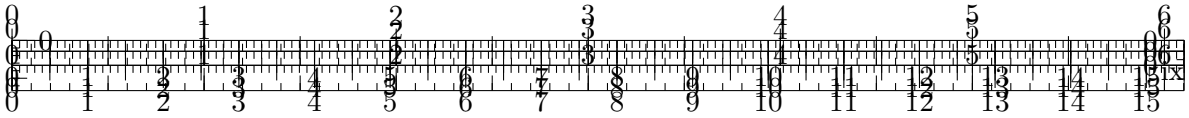

EBERHARD KARLS UNIVERSITÄT TÜBINGEN

# *Abstract*

Mathematisch-Naturwissenschaftliche Fakultät
Institut für Theoretische Physik

Master of Science

**Master thesis**

by Leopold Bodamer

This thesis investigates the application of two-dimensional photon-echo spectroscopy to model quantum systems, with a focus on open quantum system dynamics. We develop a comprehensive theoretical framework that combines the response-function formalism of nonlinear spectroscopy with master-equation approaches for open quantum systems. Starting from minimal reference models, including a single qubit and a four-level system formed by two coupled qubits, we validate our methods and apply the model to a system of $N$ qubits arranged on a cylindrical geometry, inspired by the structural motifs of microtubules. Our results demonstrate the capability of two-dimensional spectroscopy to probe coherence and energy transfer dynamics in these systems, providing insights into their quantum behavior and interactions with the environment. This work lays the groundwork for future experimental and theoretical studies in the field of quantum biology and quantum information science.

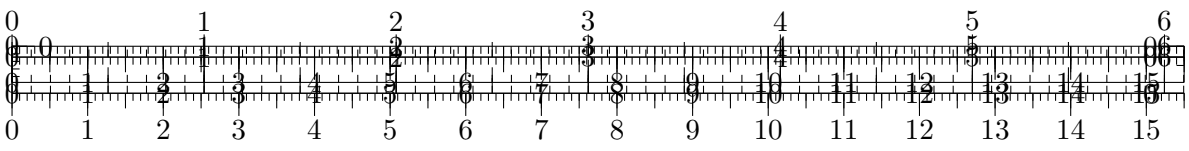

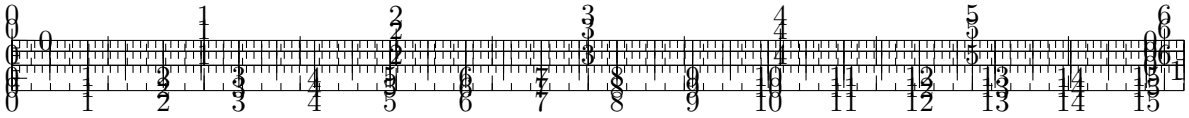

# Chapter 1

# Introduction

## 1.1 Coherence and Excitation Transport

In this chapter, we aim to explain the phenomena of long coherences (lifetimes) and the excitation transport of light on a microtubule. The proposed model takes the following approach:

- The microtubule is modeled as a cylindrical structure consisting of nodes. Each node represents an atom, which is modeled as a two-level system. The number of atoms, $N_{\text{atoms}}$, is determined by the number of chains ($n_{\text{chains}}$) and the number of rings ($n_{\text{rings}}$), assuming fixed positions for these nodes.
- The system is restricted to a single excitation.
- A time-dependent coupling to an electric field is proposed, which may be either classical or quantum in nature. This coupling is intended to facilitate spectroscopy.
- Two types of Lindblad operators are introduced to model dissipation processes. Specifically:
  1. Spontaneous decay
  2. Dephasing

The Lindblad operators introduced to model the spontaneous decay and dephasing processes for each individual atom are defined as follows:

$$C^{(i)}_{\text{decay}} = \sqrt{\gamma_0}\,\sigma^{(i)}_{-}, \tag{1.1}$$

$$C^{(i)}_{\text{dephase}} = \sqrt{\gamma_\phi}\,\sigma^{(i)}_{z}, \tag{1.2}$$

where:

- $C^{(i)}_{\text{decay}}$ describes the spontaneous decay of the $i$-th atom, with a rate given by $\gamma_0$.
- $C^{(i)}_{\text{dephase}}$ describes the dephasing of the $i$-th atom, with a rate given by $\gamma_\phi$.
- $\sigma^{(i)}_{-}$ is the lowering operator for the $i$-th atom, and $\sigma^{(i)}_{z}$ is the Pauli $z$-operator for the $i$-th atom.

**IDEA:** Give a whole introduction to quantum biology, why it is interesting, quantum consciousness, ... , microtubules, coherence, excitation transport, 2D spectroscopy, with open quantum systems

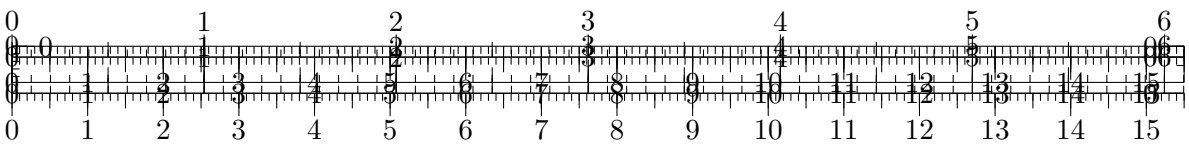

## 1.2 Motivation

It is widely assumed that one of the crucial tasks currently facing quantum theorists is to understand and characterize the behaviour of realistic quantum systems. In any experiment, a quantum system is subject to noise and decoherence due to the unavoidable interaction with its surroundings. The theory of open quantum systems aims at developing a general framework to analyze the dynamical behaviour of systems that, as a result of their coupling with environmental degrees of freedom, will no longer evolve unitarily. [36]
2DES>

**REFERENCE:** rind ref

[39], [40]
NONlinear Optics> [16], [30]
Spectroscopy investigates the interaction between matter and electromagnetic radiation, offering a means to analyze composition and structure. Central to this analysis is the understanding of how molecules respond to specific frequencies of light, revealing information about their energy levels and bonding. Key concepts include wavelength ($\lambda$), wavenumber ($\bar{\nu}$), and frequency ($\nu$). Wavelength, the distance between successive wave crests, is typically measured in nanometers or micrometers. Wavenumber, expressed in inverse centimeters ($\mathrm{cm}^{-1}$), represents the number of waves per unit distance and is directly proportional to energy, defined as $\bar{\nu} = 1/\lambda$ (where $\lambda$ is in cm). Frequency, the number of wave cycles per second, is measured in Hertz (Hz), and the angular frequency ($\omega$) is related to frequency by $\omega = 2\pi\nu$. The relationship between angular frequency and wavenumber is given by $\omega = 2\pi c\bar{\nu}$, where $c$ is the speed of light.
Next, I converted all units into femtoseconds ($fs^{-1}$), which is commonly used in time-domain spectroscopy.
Spectrometers are instruments designed to measure the intensity of light as a function of wavelength or frequency.
Different types of spectrometers are employed for various regions of the electromagnetic spectrum. Notably, UV-Vis spectrometers analyze absorption and transmission of ultraviolet and visible light, while infrared (IR) spectrometers measure the absorption of infrared light, providing insights into molecular vibrations. Nuclear Magnetic Resonance (NMR) spectrometers probe the magnetic properties of atomic nuclei, revealing molecular structure.

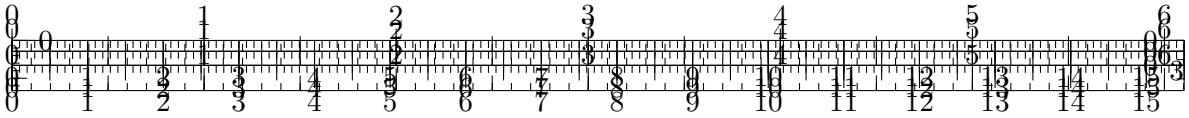

# Chapter 2

# Open Quantum Systems

## 2.1 Introduction to Open Quantum Systems

In the realm of quantum mechanics, most real-world quantum systems are not perfectly isolated. Instead, they interact with their surrounding environment, leading to the concept of *open quantum systems*. Unlike closed quantum systems that evolve unitarily according to the Schrödinger equation, open quantum systems experience non-unitary evolution due to their coupling with an external environment or reservoir. Whenever the system is driven out of equilibrium by external perturbations, this coupling makes the system relax back to equilibrium.

### 2.1.1 What are Open Quantum Systems?

Open quantum systems are quantum systems that interact with an external environment, often called a "bath," which typically has many degrees of freedom and is usually assumed to be in thermal equilibrium [6, 45]. This interaction leads to several fundamental phenomena that distinguish open systems from isolated, closed quantum systems.

A central effect is **decoherence**, where quantum superposition states lose their phase relationships due to entanglement with the environment (**dephasing**). As a result, pure quantum states evolve into classical statistical mixtures, and the system's ability to exhibit quantum interference is diminished. The characteristic time scale for this process, known as the *coherence time*, is of utmost importance in experiments, especially in high-resolution spectroscopy, quantum information processing, and quantum optics. For example, in two-dimensional electronic spectroscopy, the coherence time determines the ability to resolve quantum beats and thus extract information about energy transfer pathways in complex molecular systems [30].

In addition to dephasing, the system-environment interaction leads to **dissipation** or **thermalization**, where energy is exchanged between the system and its surroundings, causing the system to relax toward a thermal state determined by the environment's temperature.

Understanding and controlling these effects is crucial for the design of quantum technologies, such as quantum computers and sensors, where environmental noise can rapidly destroy fragile quantum states [**schlosshauer2007decoherencebook**, 23].

In summary, open quantum systems theory provides the framework to describe how quantum systems lose their "quantumness" and transition toward classical behavior due to unavoidable interactions with their environment.

### 2.1.2 Origins and Physical Motivation

Open quantum systems theory emerges naturally from the realization that perfect isolation of quantum systems is practically impossible; every quantum system in nature interacts with its environment to some degree. For instance, atoms are subject to electromagnetic field fluctuations (vacuum fluctuations) [6], quantum dots in solid-state environments couple to phonon

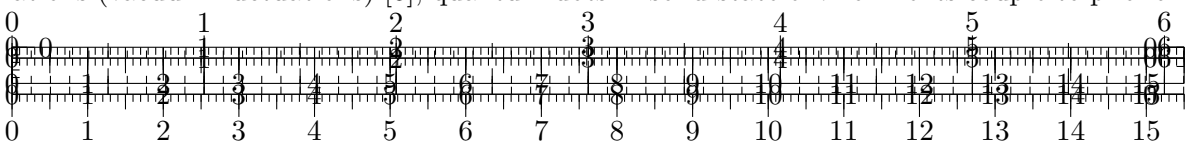

baths [45], and molecular systems interact with surrounding solvent molecules [30]. Quantum computers are particularly sensitive to environmental noise, which can rapidly destroy quantum coherence [23], while biological quantum systems such as photosynthetic complexes operate in inherently noisy cellular environments [**schlosshauer2007decoherencebook**]. These diverse scenarios all require a theoretical framework that accounts for the coexistence of quantum effects and environmental influences.

### 2.1.3 Theoretical Approaches

A variety of theoretical frameworks have been developed to describe the dynamics of open quantum systems, each with its own range of validity and underlying assumptions. The most important distinction among these approaches is whether they assume **Markovian** or **non-Markovian** dynamics.

#### Markovian vs. Non-Markovian Dynamics

**Markovian dynamics** assume that the environment has no memory: the future evolution of the system depends only on its present state, not on its past history. This is valid when the environmental correlation time is much shorter than the system's characteristic timescale. In contrast, **non-Markovian dynamics** account for memory effects, where the environment retains information about the system's past, leading to feedback and more complex evolution [6, 35].

#### Overview of Main Approaches

**Stochastic Approaches** Stochastic Schrödinger equations and quantum trajectories unravel master equations into individual pure state evolutions, clarifying measurement backaction and quantum jumps [6, 9, 44].

**Non-Markovian Approaches** Time-convolutionless and Nakajima–Zwanzig master equations introduce memory kernels to describe non-Markovian effects [6, 35]. The hierarchical equations of motion (HEOM) provide a numerically exact framework for strong coupling and non-Markovian, condensed-phase environments like liquids or solids [41]. This is the most computationally expensive method. Path-integral methods based on the Feynman–Vernon influence functional offer a non-perturbative route to non-Markovian dynamics [45].

**Master Equation Approaches** The Lindblad master equation (Markovian) gives a general form for completely positive, trace-preserving dynamics under the Markov approximation and is widely used in quantum optics and quantum information [6, 27]. The Redfield equation (Markovian but not always CPTP) follows from a microscopic Born–Markov derivation, captures dissipation and dephasing, and does not guarantee complete positivity [26, 33, 35].

**IDEA:** explain why we choose the Redfield equation for this thesis -> it represnets the best compromise between accuracy and computational efficiency for our systems of interest.

### 2.1.4 The Redfield Equation: A Central Tool

Among the various master equation approaches to open quantum systems, the Redfield equation occupies a particularly important position due to its microscopic foundation and broad applicability [6, 33]. Originally developed by A.G. Redfield in 1957 and 1965 for nuclear magnetic resonance relaxation phenomena [33], the Redfield equation describes the time evolution of the reduced density matrix of a quantum system weakly coupled to a thermal environment.

The Redfield master equation provides a systematic perturbative treatment of system-environment interactions within the Born-Markov approximation. Unlike phenomenological approaches that introduce dissipation and dephasing *ad hoc*, the Redfield formalism derives these effects directly from the microscopic Hamiltonian of the total system, making it particularly valuable for understanding the fundamental mechanisms underlying quantum decoherence [6, 45].

The key advantages of the Redfield approach include:

- **Microscopic foundation**: Derived rigorously from the von Neumann equation for the total system-environment composite, ensuring consistency with fundamental quantum mechanics [6]
- **Physical transparency**: The relaxation rates are directly related to environmental correlation functions and spectral densities, providing clear physical insight into the dissipation mechanisms [33]

However, it is important to note that the Redfield equation, while preserving trace and Hermiticity, does not guarantee complete positivity of the density matrix—a fundamental requirement for physical quantum states [36]. This limitation restricts its validity to the weak-coupling regime and requires careful analysis of its applicability in specific physical situations.

In this chapter, we will derive the Redfield equation starting from the fundamental microscopic dynamics of the system-environment composite and demonstrate how it emerges as an effective description for the reduced system dynamics. We will then examine the environmental correlation functions and spectral densities that characterize the bath properties and determine the system's relaxation behavior.

## 2.2 Derivation of the Redfield Equation from Microscopic Dynamics

The derivation of the Redfield master equation is based on open quantum theory and provides a systematic way to obtain an effective equation of motion for a quantum system coupled to an environment. This derivation follows the approach presented in [28] and can also be found in standard textbooks such as Breuer and Petruccione [6].

### 2.2.1 Setup: System + Environment

We consider a quantum system of interest interacting with a larger environment. The total system Hilbert space $\mathcal{H}_T$ is the tensor product of the system Hilbert space $\mathcal{H}_S$ and the environment Hilbert space $\mathcal{H}_E$:

$$\mathcal{H}_T = \mathcal{H}_S \otimes \mathcal{H}_E. \tag{2.1}$$

The evolution of the total system is governed by the Liouville-Von Neumann equation:

$$\dot{\rho}_T(t) = -i[H_T, \rho_T(t)], \tag{2.2}$$

where $\rho_T(t)$ is the density matrix of the total system, $H_T$ is the total Hamiltonian, and we use units where $\hbar = 1$.

The total Hamiltonian can be decomposed as:

$$H_T = H_S \otimes \mathbb{1}_E + \mathbb{1}_S \otimes H_E + \alpha H_I, \tag{2.3}$$

where:

- $H_S$ is the system Hamiltonian
- $H_E$ is the environment (bath) Hamiltonian
- $H_I$ represents the interaction between system and environment
- $\alpha$ is the coupling strength parameter

The interaction Hamiltonian is typically written in the form:

$$H_I = \sum_i S_i \otimes E_i, \tag{2.4}$$

where $S_i$ are system operators and $E_i$ are environment operators.

### 2.2.2 Reduced Dynamics and Approximations

Since we are interested in the dynamics of the system alone, we define the reduced density matrix by tracing over the environmental degrees of freedom:

$$\rho(t) = \mathrm{Tr}_E[\rho_T(t)]. \tag{2.5}$$

The exact equation of motion for $\rho(t)$ involves the full many-body dynamics of the environment, which is generally intractable. The Redfield approach provides a systematic approximation scheme by making several key assumptions:

1. **Weak coupling approximation**: The system-environment coupling is treated perturbatively (small $\alpha$)
2. **Markovian approximation**: The environment correlation time is much shorter than the system evolution time scale
3. **Born approximation**: The total state remains close to a product state $\rho_S(t) \otimes \rho_E$

The following requirements must be fulfilled by the final derived Redfield equation:

- The equation should be linear in the system density matrix $\dot{\rho}_S(t) = F(\rho_S(t))$ (reduced equation of motion).
- The equation should be Markovian, meaning that the evolution of the system density matrix at time $t$ only depends on the state of the system at time $t$ and not on its past history.
- The equation should be trace-preserving, meaning that $\mathrm{Tr}[\rho_S(t)] = \mathrm{Tr}[\rho_S(0)]$ for all times $t$.

Unlike the Lindblad equation, the Redfield equation does not guarantee the complete positivity of the density matrix, which is a requirement for a physical state. Care must be taken when determining when the Redfield equation is useful. The equation will be valid in the weak coupling limit, meaning that the coupling strength in the interaction Hamiltonian fulfills $\alpha \ll 1$.

### 2.2.3 Interaction Picture

To describe the system dynamics, we move to the interaction picture where the operators evolve with respect to $H_S + H_E$. Any arbitrary operator $O$ in the Schrödinger picture takes the form:

$$\hat{O}(t) = e^{i(H_S+H_E)t} O e^{-i(H_S+H_E)t}, \tag{2.6}$$

in the interaction picture. States now evolve only according to the interaction Hamiltonian $H_I$, and the Liouville-Von Neumann equation becomes:

$$\dot{\hat{\rho}}_T(t) = -i\alpha[\hat{H}_I(t), \hat{\rho}_T(t)], \tag{2.7}$$

which can be formally integrated as:

$$\hat{\rho}_T(t) = \hat{\rho}_T(0) - i\alpha \int_0^t ds[\hat{H}_I(s), \hat{\rho}_T(s)]. \tag{2.8}$$

Inserting this back into the equation of motion yields:

$$\dot{\hat{\rho}}_T(t) = -i\alpha \left[\hat{H}_I(t), \hat{\rho}_T(0)\right] - \alpha^2 \int_0^t \left[\hat{H}_I(t), \left[\hat{H}_I(s), \hat{\rho}_T(s)\right]\right] ds, \tag{2.9}$$

The iteration can be repeated, leading to a series expansion in powers of $\alpha$:

$$\dot{\hat{\rho}}_T(t) = -i\alpha \underbrace{\left[\hat{H}_I(t), \hat{\rho}_T(0)\right]}_{(1)} - \alpha^2 \int_0^t \underbrace{\left[\hat{H}_I(t), \left[\hat{H}_I(s), \hat{\rho}_T(s)\right]\right]}_{(2)} ds + \mathcal{O}(\alpha^3). \tag{2.10}$$

We truncate at second order, justified by the weak coupling assumption ($\alpha \ll 1$), which represents the **Born approximation**.

### 2.2.4 Partial Trace and Markovian Approximation

We assume the total system starts in a product state:

$$\hat{\rho}_T(0) = \hat{\rho}_S(0) \otimes \hat{\rho}_E(0), \tag{2.11}$$

Taking the partial trace over the environment, the first-order term vanishes if we assume $\langle E_i \rangle_0 = \mathrm{Tr}_E[E_i \hat{\rho}_E(0)] = 0$. This can always be achieved by shifting the interaction operators appropriately.

The reduced equation of motion becomes:

$$\dot{\rho}_S(t) = -\alpha^2 \int_0^t ds\, \mathrm{Tr}_E\big[\hat{H}_I(t), [\hat{H}_I(s), \hat{\rho}_S(t) \otimes \hat{\rho}_E(0)]\big]. \tag{2.12}$$

### 2.2.5 Final Redfield Equation

Substituting the interaction Hamiltonian and performing the environmental trace, we obtain:

$$\dot{\rho}_S(t) = \alpha^2 \sum_{i,j} \int_0^t ds\, C_{ij}(t-s) \left[\hat{S}_i(t), \hat{S}_j(t-s)\hat{\rho}_S(t)\right] + \text{H.c.}, \tag{2.13}$$

where the environmental correlation functions are defined as:

$$C_{ij}(\tau) = \mathrm{Tr}_E[\hat{E}_i(\tau)\hat{E}_j(0)\hat{\rho}_E(0)]. \tag{2.14}$$

This is the Redfield master equation, describing the reduced dynamics of the system under the influence of environmental correlations.

## 2.3 Environmental Correlation Functions and Spectral Properties

Having derived the Redfield equation, we now turn our attention to one of its most crucial ingredients: the characterization of the environmental properties through correlation functions and spectral densities. These quantities encode all the relevant information about how the environment affects the system dynamics and are essential for any practical application of the Redfield formalism.

The transition from the abstract mathematical framework of the Redfield equation to concrete, calculable expressions requires a detailed understanding of the bath correlation functions. These functions not only determine the strength and time scales of the system-environment interaction but also reveal the fundamental connection between quantum and classical descriptions of environmental noise.

In the following sections, we will explore how environmental correlation functions arise naturally in the Redfield framework, examine their physical interpretation, and discuss their relationship to experimentally accessible quantities such as power spectra and spectral densities. This analysis will provide the foundation for understanding how different types of environments—from thermal baths to structured reservoirs—influence quantum system dynamics.

### 2.3.1 Bath Correlation Functions

The environmental correlation functions that appear in the Redfield equation are defined as:

$$C_{ij}(\tau) = \langle E_i(\tau) E_j(0) \rangle_E, \tag{2.15}$$

where $E_i(\tau)$ represents the environment operators in the interaction picture, and $\langle \cdot \rangle_E$ denotes the expectation value with respect to the environmental state.

### 2.3.2 Physical Interpretation: Emission and Absorption Processes

A fundamental question when applying the Redfield formalism concerns whether both emission and absorption processes are correctly included in the theoretical description. This is particularly important when studying spectroscopic phenomena, where the competition between these processes determines the observed signals and the approach to thermal equilibrium.

The answer is **yes**: both spontaneous and stimulated emission, as well as thermal and induced absorption, are naturally included through the proper choice of the spectral function $S(\omega)$ that characterizes the system-environment interaction, provided this function satisfies the Kubo-Martin-Schwinger (KMS) condition for detailed balance.

The KMS condition requires that the spectral function satisfies:

$$S(-\omega) = e^{-\hbar\omega/(k_B T)} S(\omega), \tag{2.16}$$

where $T$ is the temperature of the thermal environment. This condition ensures:

- **Emission processes**: Transitions with $\omega > 0$ correspond to energy transfer from system to environment

- **Absorption processes**: Transitions with $\omega < 0$ correspond to energy transfer from environment to system
- **Detailed balance**: The ratio of forward and reverse transition rates follows the Boltzmann distribution

## 2.4 Environmental Correlation Functions and Spectral Properties

Having derived the Redfield equation, we now turn our attention to one of its most crucial ingredients: the characterization of the environmental properties through correlation functions and spectral densities. These quantities encode all the relevant information about how the environment affects the system dynamics and are essential for any practical application of the Redfield formalism.

The transition from the abstract mathematical framework of the Redfield equation to concrete, calculable expressions requires a detailed understanding of the bath correlation functions. These functions not only determine the strength and time scales of the system-environment interaction but also reveal the fundamental connection between quantum and classical descriptions of environmental noise.

In what follows, we will explore how environmental correlation functions arise naturally in the Redfield framework, examine their physical interpretation, and discuss their relationship to experimentally accessible quantities such as power spectra and spectral densities. This analysis provides the foundation for understanding how different types of environments—from thermal baths to structured reservoirs—influence quantum system dynamics.

### 2.4.1 Definition and Properties of Bath Correlation Functions

The environmental correlation functions that appear in the Redfield equation, as defined in Eq. (2.14), capture the temporal correlations in the environmental fluctuations:

$$C_{ij}(\tau) = \mathrm{Tr}_E[\hat{E}_i(\tau)\hat{E}_j(0)\hat{\rho}_E(0)]. \tag{2.17}$$

These correlation functions possess several important properties:

- **Stationarity**: For environments in thermal equilibrium, $C_{ij}(\tau)$ depends only on the time difference $\tau$, not on the absolute time
- **Hermiticity**: $C_{ij}^*(\tau) = C_{ji}(-\tau)$ due to the Hermitian nature of the environment operators
- **Decay behavior**: The correlation functions typically decay on time scales characteristic of the environmental dynamics

The spectral density, obtained through Fourier transform of the correlation function, provides complementary information about the frequency content of the environmental fluctuations:

$$S_{ij}(\omega) = \int_{-\infty}^{\infty} d\tau\, e^{i\omega\tau} C_{ij}(\tau). \tag{2.18}$$

This spectral density directly enters the Redfield rates and determines the frequency-dependent coupling between system and environment.

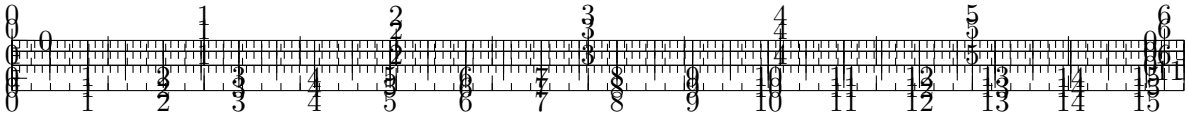

# Chapter 3

# Bath Correlation Functions and Harmonic Oscillator Environments

In the previous chapter, we derived the Redfield equation and introduced the environmental correlation functions $C_{ij}(\tau)$ that characterize the system-bath interaction. These correlation functions are central to the Redfield formalism, as they encode all the relevant information about how the environment affects the quantum system dynamics.

To make the Redfield equation practically useful, we need to specify the form of these correlation functions for realistic environmental models. In this chapter, we focus on one of the most important and widely applicable environmental models: the harmonic oscillator bath. This model captures the essential physics of many real environments, from electromagnetic field fluctuations to phonon baths in solid-state systems.

## 3.1 Bath Correlation Functions: From Theory to Practice

The general task of this chapter is to calculate the bath correlation functions that appear in the Redfield equation. These are defined as:

$$C(\tau) = \langle B(\tau)B(0)\rangle, \tag{3.1}$$

where $B$ represents the bath operators $E_i$ from the interaction Hamiltonian. This correlator measures how the operator $B$ at two different times is correlated in the thermal bath state.

For the harmonic oscillator bath model, these correlation functions can be calculated exactly, providing a solid foundation for understanding more complex environmental models. The results will show how the bath correlation functions connect to physically observable quantities such as spectral densities and how they determine the system's approach to thermal equilibrium.

## 3.2 Useful Tools

### 3.2.1 Infinite Geometric Series

An infinite geometric series is expressed as:

$$S = a + ar + ar^2 + ar^3 + \cdots = \sum_{n=0}^{\infty} ar^n, \tag{3.2}$$

where $a$ is the first term and $r$ is the common ratio. For $|r| < 1$, the sum converges to:

$$S = \frac{a}{1-r}. \tag{3.3}$$

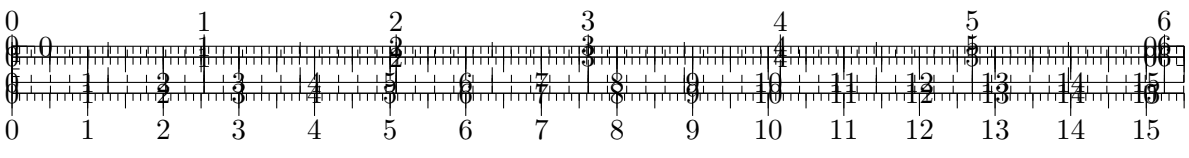

Differentiating Eq. (3.3) with respect to $r$ yields another useful series:

$$\sum_{n=0}^{\infty} n r^n = \frac{r}{(1-r)^2}, \quad \text{for } |r| < 1. \tag{3.4}$$

### 3.2.2 Trace

For a bipartite system $A \otimes B$, the reduced density matrix of system $A$ is obtained by tracing out system $B$:

$$\rho_A = \mathrm{Tr}_B[\rho_{AB}], \tag{3.5}$$

where the partial trace over the subspace $B$ is defined as:

$$\mathrm{Tr}_B \left[ \sum_{i,j,k,l} |a_i\rangle\langle a_j| \otimes |b_k\rangle\langle b_l| \right] = \sum_{i,j} |a_i\rangle\langle a_j| \mathrm{Tr}\left[|b_k\rangle\langle b_l|\right] \tag{3.6}$$

The expectation value of an operator $A$ in a system $S$ is calculated as:

$$\langle A \rangle_S = \mathrm{Tr}_S[\rho_S A] = \frac{1}{Z} \sum_n e^{-\beta E_n} A_{nn}, \tag{3.7}$$

where the inverse temperature $\beta$ is defined as:

$$\beta = \frac{1}{k_B T}. \tag{3.8}$$

## 3.3 Harmonic Oscillators

A bosonic bath is modeled by an infinitely big set of harmonic oscillators, which we assume to be in thermal equilibrium. For such a system the thermal state is described by the Gibbs distribution:

$$\rho = \frac{e^{-\beta H}}{\mathrm{Tr}\left[e^{-\beta H}\right]}, \quad H = \sum_k \hbar\omega_k \left( b_k^\dagger b_k + \frac{1}{2} \right), \quad E_k = \hbar\omega_k (n_k + \frac{1}{2}), \tag{3.9}$$

where $\omega_k$ is the frequency of the $k$-th mode, $b_k^\dagger$ and $b_k$ are the creation and annihilation operators, respectively, and $n_k = \langle b_k^\dagger b_k \rangle$ is the expectation value of the number operator. The number operator is an eigenoperator to the number states $|k\rangle$ and the number $n_k$ represents the number of excitations in that mode. The energy of the k-th mode $E_k$ is directly related to this number.

### 3.3.1 Single Mode

For a single mode $k$ harmonic oscillator $H = \hbar\omega_k b_k^\dagger b_k$ in thermal equilibrium at temperature $T$, the density matrix is given by:

$$\rho = \frac{e^{-\beta\hbar\omega_k b_k^\dagger b_k}}{Z_k}, \tag{3.10}$$

where $\omega_k$ is the constant frequency of the mode $k$. The partition function $Z$ can be calculated by the geometric series:

$$Z_k \equiv \mathrm{Tr}\left[e^{-\beta H}\right] = \sum_{m=0}^{\infty} \langle m|e^{-\beta\hbar\omega_k(n_k+\frac{1}{2})}|m\rangle \tag{3.11}$$

$$= \frac{e^{-\beta\hbar\omega_k/2}}{1-e^{-\beta\hbar\omega_k}}. \tag{3.12}$$

Using this, the expectation value of the number operator can be calculated:

$$n_k = \langle b_k^\dagger b_k\rangle_{\mathrm{th}} = \mathrm{Tr}\left[b_k^\dagger b_k \frac{e^{-\beta H}}{Z_k}\right] \tag{3.13}$$

$$= \frac{\mathrm{Tr}\left[b_k^\dagger b_k e^{-\beta\hbar\omega_k b_k^\dagger b_k}\right]}{Z_k} \tag{3.14}$$

$$= \frac{\sum_{m=0}^{\infty}\langle m|b_k^\dagger b_k e^{-\beta\hbar\omega_k b_k^\dagger b_k}|m\rangle}{\frac{e^{-\beta\hbar\omega_k/2}}{1-e^{-\beta\hbar\omega_k}}} \tag{3.15}$$

$$= \frac{e^{-\beta\hbar\omega_k}}{1-e^{-\beta\hbar\omega_k}} \tag{3.16}$$

$$= \frac{1}{e^{\beta\hbar\omega_k}-1}. \tag{3.17}$$

where we have used Eq. (3.4) in the last step. The partition function for the infinite set then generalizes to a product:

$$Z = \prod_k Z_k = \prod_k \frac{e^{-\beta\hbar\omega_k/2}}{1-e^{-\beta\hbar\omega_k}}. \tag{3.18}$$

## 3.4 Bath Correlators

Now we have enough background to actually calculate the bath correlator. In the The bath operator $B$ is defined as:

$$B = \sum_{n=1}^{\infty} c_n x_n, \tag{3.19}$$

where $c_n$ are coupling constants and $x_n$ are position operators. Note that in Sec. 2.2, the interaction Hamiltonian reduces such that only one bath correlator $C(\tau) \equiv C_{ii}(\tau)$ in Eq. (2.14) remains.

Expressing $B$ in terms of creation and annihilation operators:

$$B(0) = \sum_{n=1}^{\infty} c_n \sqrt{\frac{1}{2m_n\omega_n}}(b_n + b_n^\dagger), \tag{3.20}$$

$$B(\tau) = \sum_{n=1}^{\infty} c_n \sqrt{\frac{1}{2m_n\omega_n}}\left(b_n e^{-i\omega_n\tau} + b_n^\dagger e^{i\omega_n\tau}\right). \tag{3.21}$$

Substituting $B(\tau)$ and $B(0)$ into Eq. (3.1), we find:

$$C(\tau) = \left\langle \sum_{n=1}^{\infty} c_n \sqrt{\frac{1}{2m_n\omega_n}}(b_n e^{-i\omega_n\tau} + b_n^\dagger e^{i\omega_n\tau}) \sum_{m=1}^{\infty} c_m \sqrt{\frac{1}{2m_m\omega_m}}(b_m + b_m^\dagger) \right\rangle. \tag{3.22}$$

Similar calculations to Eq. (3.13) thermal expectation values can be calculated:

$$\langle b_n b_m^\dagger \rangle = \delta_{nm}(n_n + 1), \quad \langle b_n^\dagger b_m \rangle = \delta_{nm} n_n, \tag{3.23}$$

where $n_k$ is the Bose-Einstein distribution:

$$n_k = \frac{1}{e^{\beta\omega_k} - 1}, \tag{3.24}$$

we obtain:

$$C(\tau) = \sum_{n=1}^{\infty} \frac{c_n^2}{2m_n\omega_n} \left[ (n_n + 1)e^{-i\omega_n\tau} + n_n e^{i\omega_n\tau} \right]. \tag{3.25}$$

### 3.4.1 Spectral Density Representation

The bath correlator can be expressed in terms of the spectral density $J(\omega)$, defined as:

$$J(\omega) = \pi \sum_{n=1}^{\infty} \frac{c_n^2}{2m_n\omega_n} \delta(\omega - \omega_n). \tag{3.26}$$

With this, the bath correlator becomes:

$$C(\tau) = \int_0^{\infty} d\omega \frac{J(\omega)}{\pi} \left[ (n(\omega) + 1)e^{-i\omega\tau} + n(\omega)e^{i\omega\tau} \right]. \tag{3.27}$$

### 3.4.2 Continuum Limit

As the frequencies $\{\omega_j\}$ become dense, the sum transitions to an integral:

$$\sum_{j=1}^{\infty} \quad \longrightarrow \quad \int d\omega' \, \rho(\omega'),$$

where $\rho(\omega')$ is the density of states. The coupling $g_j$ becomes a function of frequency, $g(\omega')$, leading to:

$$J(\omega) = \rho(\omega)\, g(\omega)^2.$$

In this continuum limit, the bath correlator Eq. (3.25) becomes:

$$C(\tau) = \int_0^{\infty} d\omega \frac{J(\omega)}{\pi} \left[ \coth\left(\frac{\beta\omega}{2}\right) \cos(\omega\tau) - i \sin(\omega\tau) \right]. \tag{3.28}$$

### 3.4.3 Ohmic Spectral Density

Source: Ulrich Weiss chapter 7.3: (*my interpretation: The Redfield equation is influenced by classical phenomenological models of dissipation*) For an Ohmic spectral density, the damping is frequency-independent, and the spectral density is given by:

$$J(\omega) \propto \gamma\omega, \tag{3.29}$$

where $\gamma$ is the damping constant. To ensure physical behavior, a cutoff is introduced:

$$J(\omega) = \eta \frac{\omega^s}{\omega_c^{s-1}} e^{-\omega/\omega_c}, \tag{3.30}$$

where $\eta$ is a dimensionless coupling constant, $\omega_c$ is the cutoff frequency, and $s$ determines the type of spectral density (Ohmic for $s = 1$, sub-Ohmic for $s < 1$, and super-Ohmic for $s > 1$).

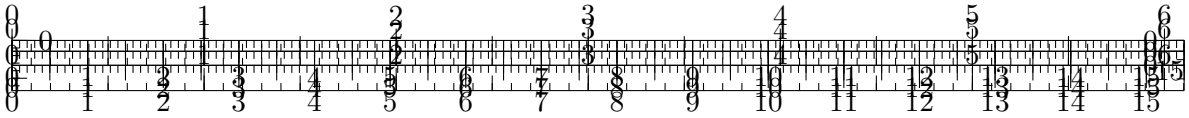

# Chapter 4

# Numerical Implementation of Two-Dimensional Electronic Spectroscopy

This chapter presents the computational framework developed for simulating two-dimensional electronic spectroscopy (2DES) spectra of molecular systems. The implementation focuses on the technical aspects of quantum system evolution, pulse sequence generation, data processing, and visualization, providing a bridge between the theoretical framework established in previous chapters and practical computational methods.

## 4.1 Overview of Simulation Architecture

The simulation framework follows a modular structure that separates quantum mechanical evolution from spectroscopic data processing. The general workflow consists of:

1. Definition of quantum system parameters (energy levels, dipole moments, coupling strengths)
2. Generation of pulse sequences with specific time delays and phases
3. Evolution of the density matrix under pulse influences and environmental coupling
4. Calculation of the system's polarization response
5. Processing of time-domain data to obtain frequency-domain 2D spectra
6. Averaging over inhomogeneous distributions and phase cycling

This modular approach enables systematic investigation of different physical parameters while maintaining computational efficiency through parallel processing capabilities.

## 4.2 Computing Two-Dimensional Polarization Response

The core calculation computes the third-order polarization response by iterating through coherence times ($t_{\text{coh}}$) and detection times ($t_{\text{det}}$) for a given waiting time ($T_{\text{wait}}$):

$$P^{(3)}(t_{\text{coh}}, T_{\text{wait}}, t_{\text{det}}) = \text{Tr}[\hat{\mu} \cdot \hat{\rho}^{(3)}(t_{\text{coh}}, T_{\text{wait}}, t_{\text{det}})] \tag{4.1}$$

where $\hat{\mu}$ is the dipole operator and $\hat{\rho}^{(3)}$ is the third-order density matrix. This calculation implements the three-pulse sequence through sequential evolution steps:

1. Apply the first pulse with phase $\phi_0$ and evolve for coherence time $t_{\text{coh}}$

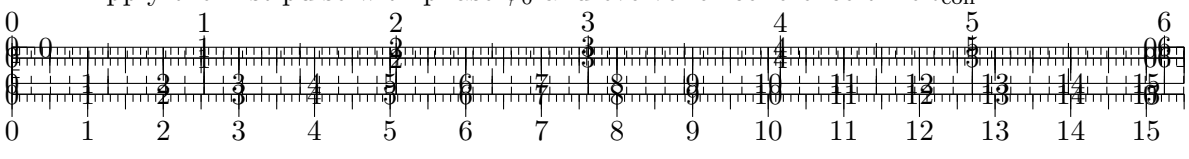

2. Apply the second pulse with phase $\phi_1$ and evolve for waiting time $T_{\text{wait}}$
3. Apply the third pulse with phase $\phi_2$ and measure response during detection time $t_{\text{det}}$

The temporal evolution utilizes either custom equations derived from literature or standard quantum dynamics solvers from the QuTiP [24] library, ensuring both flexibility and computational accuracy.

## 4.3 Inhomogeneous Broadening Implementation

To accurately model molecular systems, the simulation accounts for inhomogeneous broadening by averaging over a distribution of transition frequencies. The distribution follows a Gaussian profile:

$$\sigma(E - E_0) = \frac{1}{\sigma_{\text{val}}\sqrt{2\pi}} \exp\left(-\frac{(E - E_0)^2}{2\sigma_{\text{val}}^2}\right) \tag{4.2}$$

where $\sigma_{\text{val}} = \Delta/(2\sqrt{2\ln 2})$ relates the standard deviation to the full width at half maximum $\Delta$.
The sampling from this distribution employs a rejection sampling algorithm that ensures accurate representation of the broadening profile while maintaining computational efficiency. The algorithm operates by:

1. Defining the sampling range $[E_{\min}, E_{\max}] = [E_0 - E_{\text{range}} \cdot \Delta, E_0 + E_{\text{range}} \cdot \Delta]$
2. Computing the maximum value $\sigma_{\max}$ of $\sigma(E)$ in the range
3. Generating candidate values uniformly and accepting them based on the probability density
4. Repeating until the desired number of samples is obtained

## 4.4 Parallel Processing of Parameter Combinations

The computationally intensive nature of 2DES simulations, particularly when averaging over frequency samples and phase combinations, necessitates efficient parallel processing. The averaged response is calculated as:

$$\langle P^{(3)}(t_{\text{coh}}, T_{\text{wait}}, t_{\text{det}})\rangle = \frac{1}{N_\omega N_\phi} \sum_{i=1}^{N_\omega} \sum_{j=1}^{N_\phi} P^{(3)}_{\omega_i,\phi_j}(t_{\text{coh}}, T_{\text{wait}}, t_{\text{det}}) \tag{4.3}$$

where $N_\omega$ represents the number of frequency samples and $N_\phi$ the number of phase combinations. The implementation utilizes Python's `ProcessPoolExecutor` to distribute calculations across available CPU cores, significantly reducing computation time for parameter sweeps.

## 4.5 Fourier Transformation and Spectral Analysis

The conversion from time-domain to frequency-domain spectra utilizes two-dimensional Fourier transformation:

$$S(\omega_{\text{coh}}, \omega_{\text{coh}}) = \int_{-\infty}^{\infty}\int_{-\infty}^{\infty} E^{(3)}_{\vec{k}_S}(t_{\text{coh}}, T, t) e^{-i\omega_{\text{coh}} t_{\text{coh}}} e^{-i\omega_{\text{coh}} t_{\text{coh}}}\, dt_{\text{coh}}\, dt \tag{4.4}$$

In the discrete implementation, this becomes a Fast Fourier Transform (FFT) operation:

$$S[k,l] = \sum_{m=0}^{M-1} \sum_{n=0}^{N-1} P^{(3)}[m,n] \exp\left(-i\frac{2\pi km}{M}\right) \exp\left(-i\frac{2\pi ln}{N}\right) \tag{4.5}$$

The frequency axes are converted to wavenumber units ($10^4$ cm$^{-1}$) using:

$$\nu = \frac{f}{c} \times 10^4 \text{ cm}^{-1} \tag{4.6}$$

where $f$ is the frequency in cycles/fs and $c = 2.998 \times 10^{-5}$ cm/fs is the speed of light.

## 4.6 Data Processing and Visualization

The 2D spectra visualization system represents different aspects of the complex-valued data:

- Real part: Absorptive component containing peak positions
- Imaginary part: Dispersive component providing line shape information
- Absolute value: Overall signal strength
- Phase: Phase relationship between excitation and detection processes

For data containing both positive and negative values, a custom white-centered colormap enhances visualization of signal features. The normalization scheme:

$$\text{data}_{\text{normalized}} = \frac{\text{data}}{\max(|\text{data}|)} \tag{4.7}$$

ensures consistent visualization across different parameter sets while preserving relative signal amplitudes.

## 4.7 Extending Time and Frequency Axes

To improve Fourier transform resolution and reduce artifacts from finite sampling, the implementation supports zero-padding of time-domain data:

$$\text{data}_{\text{extended}} = \begin{bmatrix} 0 & \cdots & 0 & \text{data} & 0 & \cdots & 0 \end{bmatrix} \tag{4.8}$$

The corresponding time axes extend proportionally:

$$t_{\text{extended}} = \{t_0 - n_{\text{pre}}\Delta t, \ldots, t_0, \ldots, t_N, \ldots, t_N + n_{\text{post}}\Delta t\} \tag{4.9}$$

where $n_{\text{pre}}$ and $n_{\text{post}}$ represent the number of zero-padded points before and after the original data.

## 4.8 Global Data Combination for Multiple Waiting Times

For studies of temporal evolution in coherence phenomena, the simulation supports scanning over multiple waiting times. The local time and frequency data are mapped to global axes through:

$$\text{global\_data}[\text{idx}_{t_{\text{coh}}}, \text{idx}_t] += \text{local\_data}[\text{local\_idx}_{t_{\text{coh}}}, \text{local\_idx}_t] \tag{4.10}$$

where $\text{idx}_{t_{\text{coh}}}$ and $\text{idx}_t$ represent indices in the global arrays corresponding to local values of $t_{\text{coh}}$ and $t_{\text{det}}$. The global data normalization:

$$\text{global\_data}_{\text{normalized}} = \frac{\text{global\_data}}{N_{T_{\text{wait}}}} \tag{4.11}$$

produces the average spectrum over all waiting times, enabling analysis of relaxation and dephasing processes.

## 4.9 Connection to Theoretical Framework

The numerical implementation directly implements the theoretical concepts established in previous chapters:

- Quantum system evolution follows the Redfield master equation for open quantum systems (Chapter 2)
- Polarization calculations implement the nonperturbative approach for 2DES theory
- Spectral analysis methods extract signatures of quantum coherence in biological systems
- Environmental coupling effects are incorporated through systematic parameter studies

This computational framework provides a robust platform for simulating 2DES spectra of complex molecular systems and extracting quantum dynamical parameters relevant to biological function.

## 4.10 Validation and Performance Considerations

The implementation includes validation procedures comparing simulation results against analytical solutions for simple systems. Performance optimization through vectorized operations and parallel processing enables parameter sweeps necessary for comprehensive system characterization.
Special considerations for biological systems include:

1. Larger inhomogeneous broadening due to complex environments
2. Faster dephasing from environmental coupling
3. Multiple chromophore contributions to the signal
4. Energy transfer processes on various timescales

The simulation framework accommodates these aspects through customizable system parameters and flexible averaging procedures, providing a versatile tool for investigating quantum coherence phenomena in biological systems.

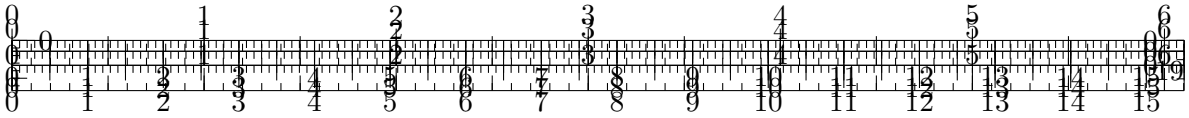

# Chapter 5

# Principles of Spectroscopy

## 5.1 Fundamentals of Spectroscopy

Spectroscopy, in its broadest definition, is the study of the interaction between matter and electromagnetic radiation as a function of wavelength or frequency [30]. This powerful analytical technique provides insights into the composition, structure, and dynamics of physical systems by examining how they absorb, emit, or scatter light. The fundamental principle underlying all spectroscopic methods is that each atom, molecule, or complex system has a unique set of energy levels, and transitions between these levels involve the absorption or emission of photons with specific energies

**REFERENCE:** find better source

[4].

### 5.1.1 Basic Principles

The foundation of spectroscopy rests on the quantization of energy in atomic and molecular systems. According to quantum mechanics, atoms and molecules can exist only in discrete energy states [2]. The energy difference between two states, $\Delta E$, determines the frequency $\nu$ or wavelength $\lambda$ of light that can be absorbed or emitted during a transition between these states, following Planck's relation:

$$\Delta E = h\nu = \frac{hc}{\lambda} \tag{5.1}$$

where $h$ is Planck's constant and $c$ is the speed of light. This relation forms the basis for spectroscopic analysis, allowing researchers to probe the energy structure of matter by observing the spectrum of absorbed or emitted radiation.

### 5.1.2 Characterization of Electromagnetic Radiation

A monochromatic plane electromagnetic wave in free space (vacuum) may be written in one spatial dimension (propagation along $z$) as

$$E(z,t) = E_0 \cos(kz - \omega t + \phi) \tag{5.2}$$

where $E_0$ is the (real) amplitude, $\phi$ a constant phase, $k$ the magnitude of the wavevector (spatial angular frequency), and $\omega$ the angular frequency. The fundamental kinematic relations for propagation in vacuum are

$$\omega = 2\pi\nu, \qquad k = \frac{2\pi}{\lambda}, \qquad \lambda = \frac{c}{\nu} = \frac{2\pi c}{\omega} \tag{5.3}$$

with $\nu$ the (cycle) frequency in hertz (Hz), $\lambda$ the wavelength in metres (m), and $c$ the speed of light in vacuum. In a material medium the phase velocity is $v_p = c/n(\nu)$ and $\lambda$ is replaced by $\lambda_n = v_p/\nu = \lambda/n(\nu)$, where $n(\nu)$ is the refractive index.

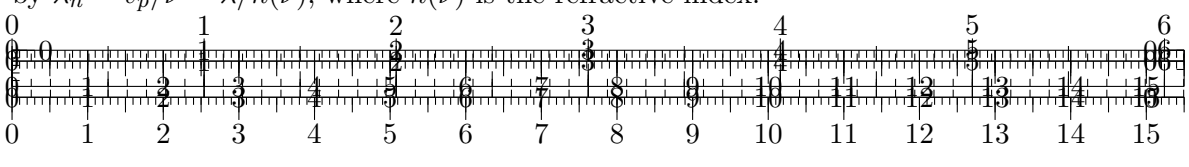

Two closely related but distinct reciprocal spatial quantities are used in spectroscopy and should not be conflated:

- The *wavevector magnitude* $k = 2\pi/\lambda$ (units $\mathrm{m}^{-1}$), which appears explicitly in the plane wave phase $kz$.
- The *(spectroscopic) wavenumber* $\tilde{\nu}$, defined conventionally as the reciprocal wavelength expressed in centimetres:

$$\tilde{\nu} = \frac{1}{\lambda_{(\mathrm{cm})}} = \frac{1}{\lambda/\mathrm{cm}} \quad [\mathrm{cm}^{-1}]. \tag{5.4}$$

  It follows that $\tilde{\nu} = 10^{-2}/\lambda$ when $\lambda$ is given in metres.

The notation $\nu$ (Greek letter nu) is widely used for the frequency (Hz). To avoid ambiguity we use a tilde for the spectroscopic wavenumber: $\tilde{\nu}$. The energetic content of radiation can be expressed equivalently using any of the variables above:

$$E = h\nu = \hbar\omega = hc\,\tilde{\nu} \tag{5.5}$$

with $h$ Planck's constant and $\hbar = h/2\pi$. Equation (5.5) is a restatement of Eq. (5.1) using alternative spectral variables.
Useful unit conversions (exact in the SI or by definition) frequently encountered in spectroscopy are:

$$1\,\mathrm{nm} = 10^{-9}\,\mathrm{m}, \qquad 1\,\mu\mathrm{m} = 10^{-6}\,\mathrm{m}, \qquad 1\,\text{Å} = 10^{-10}\,\mathrm{m}, \tag{5.6}$$

$$1\,\mathrm{cm}^{-1} \approx 29.9792458\,\mathrm{GHz}, \qquad 1\,\mathrm{cm}^{-1} \approx 1.23984198 \times 10^{-4}\,\mathrm{eV}. \tag{5.7}$$

The gigahertz conversion uses $c = 2.99792458 \times 10^{10}\,\mathrm{cm\,s}^{-1}$; the electronvolt conversion uses Eq. (5.5) and $1\,\mathrm{eV} = 1.602176634 \times 10^{-19}\,\mathrm{J}$.

**Spectral Regions and Notation** Spectral domains are commonly quoted in either wavelength $\lambda$ or (spectroscopic) wavenumber $\tilde{\nu}$ to avoid large powers of ten. Representative vacuum ranges are (non-unique boundaries): microwave ($\tilde{\nu} \lesssim 10\,\mathrm{cm}^{-1}$), terahertz ($\sim$ 10–100 $\mathrm{cm}^{-1}$), mid-infrared ($\sim$ 400–4000 $\mathrm{cm}^{-1}$), near-infrared ($\sim$ 4000–12500 $\mathrm{cm}^{-1}$), visible ($\sim$ 12500–25000 $\mathrm{cm}^{-1}$; 800–400 nm), ultraviolet ($\gtrsim 25000\,\mathrm{cm}^{-1}$). Exact numerical cutoffs vary slightly between sources. The linear relation $E = hc\tilde{\nu}$ (cf. Eq. (5.5)) makes $\tilde{\nu}$ a convenient axis for comparing transition energies.

**Remark on Re-Emission** Following absorption, isotropic spontaneous re-emission (radiative relaxation) redistributes photon directions so that only a negligible fraction re-enters the forward detection solid angle, yielding a net attenuation of the incident beam while preserving the possibility of repeated absorption events. The corresponding emission (fluorescence / phosphorescence) spectra, arising from these radiative pathways, will be exploited later in this work for extracting dynamical information from heterodyne-detected emitted fields.
Finally, we remark that $\tilde{\nu}$ (in $\mathrm{cm}^{-1}$) is a convenient linear measure of photon energy, since differences $\Delta\tilde{\nu}$ correspond directly to energy gaps $\Delta E = hc\,\Delta\tilde{\nu}$ without requiring explicit factors of $2\pi$.

### 5.1.3 Classification of Spectroscopic Techniques

Spectroscopic methods can be categorized based on various criteria:

- **Nature of the interaction:** Absorption, emission, scattering, reflection

- **Frequency range:** Radio-frequency, microwave, terahertz, infrared, visible, ultraviolet, X-ray, gamma-ray
- **Type of energy transition:** Electronic, vibrational, rotational, nuclear
- **Number of photons involved:** Linear (one-photon) vs. nonlinear (multi-photon) spectroscopy

Each spectroscopic technique provides different information about the system under study. For instance, rotational spectroscopy reveals molecular geometry, vibrational spectroscopy elucidates bonding patterns, and electronic spectroscopy probes electronic structure and excited state dynamics.

### 5.1.4 Energy-Dependent Molecular Interactions

The energy of electromagnetic radiation determines the type of molecular motion or electronic transition that can be induced. According to Planck's relation,

$$\Delta E = h\nu = \frac{hc}{\lambda} \tag{5.8}$$

higher frequency radiation carries more energy per photon, enabling interactions with progressively higher-energy molecular degrees of freedom [4, 30].
The electromagnetic spectrum can be systematically understood in terms of increasing photon energy and the corresponding molecular responses:

- **Microwave radiation** possesses the lowest energy among the spectroscopically relevant regions and primarily affects the rotational motion of molecules. The energy scale ($\sim 10^{-5}$ to $10^{-3}$ eV) matches typical rotational energy level spacings in gas-phase molecules. Microwave absorption causes molecules to undergo transitions between rotational states, increasing their angular momentum. This principle underlies the operation of microwave ovens, where 2.45 GHz radiation induces rotational motion in water molecules, generating heat through molecular agitation.
- **Infrared (IR) radiation** carries higher energy than microwave radiation and couples to vibrational motion within molecules. The photon energies ($\sim 10^{-3}$ to 1 eV) correspond to typical vibrational quanta in molecules. When absorbed, IR radiation excites molecular vibrations, causing bonds to stretch, bend, or undergo more complex deformation modes. This selectivity makes IR spectroscopy a powerful tool for identifying chemical functional groups and studying molecular dynamics.
- **Visible light** possesses sufficient energy ($\sim$ 1.5 to 3 eV) to promote electronic transitions, moving electrons from occupied orbitals to higher-energy unoccupied states. Upon electronic excitation, molecules often exhibit fluorescence or phosphorescence as electrons return to lower energy states, emitting photons in the process. This electronic excitation forms the basis of photochemistry and photobiology.
- **Ultraviolet (UV) radiation** carries even higher energy ($\sim$ 3 to 12 eV) and can induce high-energy electronic transitions. At sufficient intensities, UV radiation possesses enough energy to break covalent bonds directly, leading to photodissociation processes. This is exemplified by the UV-induced decomposition of ozone ($O_3$) in the stratosphere, where UV photons break the O-O bonds, playing a crucial role in atmospheric chemistry.

This energy hierarchy demonstrates why spectroscopic techniques using different frequency ranges provide complementary information about molecular structure and dynamics. The systematic increase in photon energy enables probing of molecular systems from their lowest-energy rotational modes to high-energy electronic excitations and bond-breaking processes.

### 5.1.5 Energy Dissipation After Absorption

After a molecule absorbs a photon of energy $E = h\nu$ its energy must be redistributed or released; otherwise continuous irradiation would rapidly saturate all accessible states. Experimentally, ordinary samples exhibit persistent absorption bands under prolonged illumination, demonstrating that excited molecules relax efficiently. Two principal classes of de-excitation pathways operate:

- **Non-radiative (thermal) relaxation:** Collisional (vibrational) energy transfer to surrounding molecules leads to rapid conversion of excess internal energy into lattice / solvent kinetic energy (heating). This typically proceeds through intramolecular vibrational redistribution followed by intermolecular energy transfer.
- **Radiative relaxation:** Spontaneous emission (fluorescence or phosphorescence, depending on spin manifold) returns population to lower electronic (and vibrational) states with emission of photons of characteristic frequencies. The emitted photons are (for an isotropic medium without cavity structuring) distributed nearly isotropically, so only a small solid angle fraction reaches a forward detector aligned with the incident collimated beam, yielding a net attenuation (absorption) of the directed beam intensity despite re-emission events.

Consequently, an absorption spectrum records the net loss from the incident mode; re-emitted photons largely populate other directions (or are spectrally shifted). The corresponding emission spectra (steady-state or time-resolved) provide complementary information on excited-state structure, relaxation cascades, and will play an important role in later parts of this work where emitted (heterodyne-detected) fields are analysed.

### 5.1.6 Time Scales in Spectroscopy

Different spectroscopic methods operate on different time scales, allowing the investigation of processes ranging from ultrafast electronic motions to slow conformational changes [3, 13]:

- Femtosecond ($10^{-15}$ s): Electronic transitions, vibrational coherences
- Picosecond ($10^{-12}$ s): Vibrational relaxation, rotational motion
- Nanosecond ($10^{-9}$ s): Fluorescence lifetimes, energy transfer
- Microsecond to millisecond ($10^{-6}$ to $10^{-3}$ s): Chemical reactions, protein folding

The development of ultrafast laser systems has revolutionized spectroscopy by allowing direct observation of molecular dynamics on femtosecond time scales, leading to the field of femtochemistry and ultrafast spectroscopy.

### 5.1.7 Macroscopic Samples and Collective Dipolar Oscillations

When considering spectroscopic measurements on macroscopic samples, it is essential to understand how individual molecular responses combine to produce observable signals. In a typical spectroscopic experiment, the sample contains on the order of Avogadro's number

($\sim 10^{23}$) of molecules, each potentially acting as an oscillating electric dipole when interacting with electromagnetic radiation [12].
The collective behavior of these molecular dipoles determines the macroscopic polarization of the sample. When an external electromagnetic field is applied, individual molecules undergo dipole transitions, creating time-varying dipole moments. The coherent superposition of these individual dipolar oscillations produces a macroscopic polarization wave that can propagate through the medium and be detected experimentally.
The macroscopic polarization $\vec{P}(\vec{r},t)$ arises from the spatial and temporal averaging of microscopic dipole moments $\vec{\mu}_i(t)$ over the sample volume:

$$\vec{P}(\vec{r},t) = \frac{1}{V}\sum_i \vec{\mu}_i(t)\delta(\vec{r}-\vec{r}_i) \tag{5.9}$$

where $V$ is the sample volume, $\vec{r}_i$ is the position of the $i$-th molecule, and the sum extends over all molecules in the interaction region. This macroscopic polarization acts as a source term in Maxwell's equations, generating the electromagnetic fields that constitute the spectroscopic signal.
The phase relationships between individual dipolar oscillations are crucial for understanding spectroscopic line shapes and signal intensities. In the case of inhomogeneously broadened systems, different molecules oscillate at slightly different frequencies due to variations in their local environment. The resulting dephasing of individual oscillators leads to the characteristic decay of macroscopic coherences observed in techniques such as photon echo spectroscopy [30].
This collective dipolar response provides the fundamental link between microscopic quantum mechanical processes in individual molecules and the macroscopic electromagnetic fields measured in spectroscopic experiments. Understanding this connection is essential for the quantitative interpretation of spectroscopic data and the extraction of molecular-level information from ensemble measurements [12].

## 5.2 Nonlinear Optics

Nonlinear optics deals with phenomena that occur when the response of a material to an applied optical field depends nonlinearly on the strength of the field [5]. This nonlinearity becomes significant at high light intensities, such as those provided by pulsed lasers.

### 5.2.1 Linear vs. Nonlinear Optical Response

In the linear regime, the induced polarization $\vec{P}$ in a material is directly proportional to the applied electric field $\vec{E}$:

$$\vec{P} = \varepsilon_0 \chi^{(1)} \vec{E} \tag{5.10}$$

where $\varepsilon_0$ is the vacuum permittivity and $\chi^{(1)}$ is the linear susceptibility tensor. This relationship describes phenomena such as refraction and absorption.
In the nonlinear regime, the polarization can be expressed as a power series in the electric field:

$$\vec{P} = \varepsilon_0(\chi^{(1)}\vec{E} + \chi^{(2)}\vec{E}^2 + \chi^{(3)}\vec{E}^3 + \ldots) \tag{5.11}$$

where $\chi^{(2)}$ and $\chi^{(3)}$ are the second- and third-order nonlinear susceptibility tensors, respectively. These higher-order terms give rise to a variety of nonlinear optical phenomena.

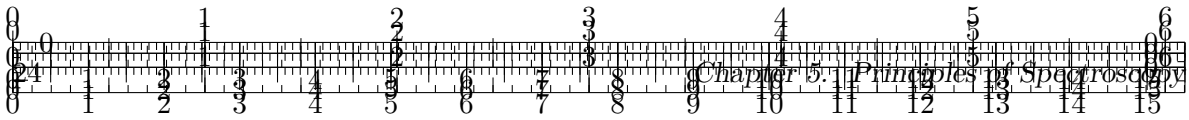


### 5.2.2 Second-Order Nonlinear Processes

Second-order nonlinear processes, governed by the $\chi^{(2)}$ term, occur only in noncentrosymmetric materials, which lack inversion symmetry. Important second-order effects include:

- **Second Harmonic Generation (SHG):** Two photons of frequency $\omega$ combine to generate a photon of frequency $2\omega$.
- **Sum Frequency Generation (SFG):** Two photons of frequencies $\omega_1$ and $\omega_2$ combine to produce a photon of frequency $\omega_1 + \omega_2$.
- **Difference Frequency Generation (DFG):** Two photons of frequencies $\omega_1$ and $\omega_2$ interact to create a photon of frequency $\omega_1 - \omega_2$.
- **Optical Parametric Amplification (OPA):** A pump photon of frequency $\omega_p$ splits into signal ($\omega_s$) and idler ($\omega_i$) photons, such that $\omega_p = \omega_s + \omega_i$.

### 5.2.3 Third-Order Nonlinear Processes

Third-order nonlinear processes, governed by the $\chi^{(3)}$ term, can occur in all materials, regardless of symmetry. Key third-order effects include:

- **Third Harmonic Generation (THG):** Three photons combine to generate a photon of tripled frequency.
- **Four-Wave Mixing (FWM):** Four photons interact, satisfying energy conservation.
- **Nonlinear Refraction:** The refractive index depends on light intensity (Kerr effect).
- **Two-Photon Absorption (TPA):** Simultaneous absorption of two photons to excite a transition.

These third-order processes form the basis for many nonlinear spectroscopic techniques, including pump-probe spectroscopy, transient grating, and various multidimensional spectroscopies.

### 5.2.4 Four-Level System Model for Third-Order Spectroscopy

The four-level system represents the minimal complete model for describing third-order nonlinear spectroscopic phenomena [1, 10]. While simpler models such as two-level systems (TLS) are sufficient for understanding linear spectroscopy and some basic nonlinear effects, they cannot fully capture all pathways contributing to third-order signals like those in 2D electronic spectroscopy or photon echo experiments.
In a typical four-level system, the energy states include:

- $|g\rangle$: Ground state
- $|e_1\rangle$ and $|e_2\rangle$: First excited states (single excitons)
- $|f\rangle$: Doubly excited state (two excitons)

This configuration allows modeling of all possible Liouville pathways that contribute to the third-order response function [30]. The inclusion of multiple excited states and a doubly excited state is essential for describing phenomena such as ground-state bleaching, stimulated emission, and excited-state absorption—the three primary components of signals observed in techniques like transient absorption and 2D electronic spectroscopy.

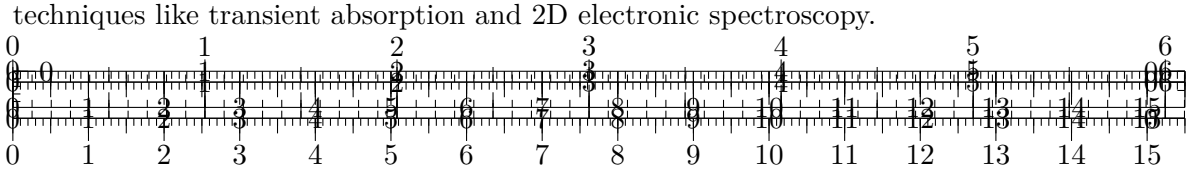

The third-order polarization $P^{(3)}$ in such a system can be expressed as a sum of different pathways:

$$P^{(3)} = P^{(3)}_{GSB} + P^{(3)}_{SE} + P^{(3)}_{ESA} + \dots \tag{5.12}$$

where GSB, SE, and ESA represent ground-state bleaching, stimulated emission, and excited-state absorption, respectively. The line-broadening function formalism within this four-level model enables detailed analysis of spectral lineshapes and system-bath interactions [1, 10]. While two-level systems are pedagogically valuable and simplify certain calculations, the four-level model captures the richness of nonlinear spectroscopic signals and serves as the foundation for interpreting complex experiments such as multidimensional spectroscopy.

### 5.2.5 Optical Bloch Equations

The interaction of light with matter in nonlinear spectroscopy is often described using the density matrix formalism and the optical Bloch equations [42]. For a simple two-level system, the density matrix elements $\rho_{ij}$ evolve according to:

$$\frac{d\rho_{11}}{dt} = -i\frac{\mu_{12}E(t)}{\hbar}(\rho_{21} - \rho_{12}) - \Gamma_1\rho_{11} \tag{5.13}$$

$$\frac{d\rho_{12}}{dt} = -i\omega_{12}\rho_{12} - i\frac{\mu_{12}E(t)}{\hbar}(\rho_{22} - \rho_{11}) - \Gamma_2\rho_{12} \tag{5.14}$$

where $\omega_{12}$ is the transition frequency, $\mu_{12}$ is the transition dipole moment, $E(t)$ is the electric field, and $\Gamma_1$ and $\Gamma_2$ are the population relaxation and decoherence rates, respectively. These equations can be extended to describe more complex systems and higher-order nonlinear responses.

## 5.3 Wavevector Phase-Matching Conditions

Phase-matching is a crucial concept in nonlinear optics that determines the efficiency and directionality of nonlinear optical processes [5],

**REFERENCE:** find ref Scheurer2001

. It ensures that the generated signal field constructively interferes throughout the interaction medium.

### 5.3.1 Physical Meaning of Phase-Matching

In nonlinear optical processes, multiple light waves interact within a material to generate new frequencies. For these processes to be efficient, the phase relationship between the interacting waves must be maintained throughout the propagation distance. This condition is known as phase-matching.
Physically, phase-matching represents momentum conservation in the photon picture. For a general nonlinear process, the wavevector of the generated signal ($\vec{k}_s$) is determined by the vector sum of the input wavevectors:

$$\vec{k}_s = \pm\vec{k}_1 \pm \vec{k}_2 \pm \vec{k}_3 \pm \dots \tag{5.15}$$

The signs depend on whether the corresponding field acts as a "bra" ($-$) or a "ket" ($+$) in the quantum mechanical description, which corresponds to photon emission or absorption, respectively.

### 5.3.2 Phase-Matching in Four-Wave Mixing

Four-wave mixing (FWM) is a third-order nonlinear process that plays a central role in many spectroscopic techniques. In a typical FWM experiment, three input fields with wavevectors $\vec{k}_1$, $\vec{k}_2$, and $\vec{k}_3$ generate a signal in the direction $\vec{k}_s$ given by:

$$\vec{k}_s = \pm\vec{k}_1 \pm \vec{k}_2 \pm \vec{k}_3 \tag{5.16}$$

Different combinations of signs correspond to different phase-matching conditions, leading to signals in different spatial directions. These distinct signal directions allow separation of various nonlinear optical processes.

### 5.3.3 Rephasing and nonrephasing Signals

In the context of multidimensional spectroscopy, phase-matched signals are often classified into rephasing and nonrephasing contributions [10, 20]:

- **Rephasing signals** follow the phase-matching condition $\vec{k}_s = -\vec{k}_1+\vec{k}_2+\vec{k}_3$. During the evolution period between the first and second interactions, the phase accumulated due to different frequencies can be reversed during the period between the third interaction and signal emission. This leads to a photon echo effect.
- **nonrephasing signals** satisfy $\vec{k}_s = +\vec{k}_1 - \vec{k}_2 + \vec{k}_3$. In this case, the phase evolution continues in the same direction, and no echo is formed.

The combination of rephasing and nonrephasing signals provides comprehensive information about the system's energy structure and dynamics.

### 5.3.4 Phase Cycling in Nonlinear Spectroscopy

While phase-matching enables the spatial isolation of desired nonlinear signals, phase cycling provides an alternative or complementary approach by distinguishing signals based on their phase characteristics rather than their spatial propagation directions

**REFERENCE:** find ref

This technique is particularly valuable in experiments where spatial isolation is impractical, such as in collinear beam geometries or when studying samples with significant scattering. In phase cycling, multiple measurements are taken with systematically varied phases of the excitation pulses. The desired nonlinear signals can then be extracted through appropriate linear combinations of these measurements. The fundamental principle relies on the fact that different nonlinear pathways respond distinctly to changes in the phases of the input fields. For a third-order signal generated by three excitation pulses with phases $\phi_1$, $\phi_2$, and $\phi_3$, the phase of the resulting signal depends on the specific pathway:

$$\phi_s = \pm\phi_1 \pm \phi_2 \pm \phi_3 \tag{5.17}$$

By varying the input phases through a complete cycle (typically in steps of $\pi/2$) and applying discrete Fourier transform methods to the collected data, specific pathways can be isolated based on their unique phase dependencies.

A common implementation is the 4-step phase cycling procedure, where each input pulse phase is cycled through values of $\{0, \pi/2, \pi, 3\pi/2\}$. For three-pulse experiments, this results in 64 possible phase combinations, although in practice, a reduced set is often sufficient to isolate signals of interest.

Phase cycling offers several advantages:

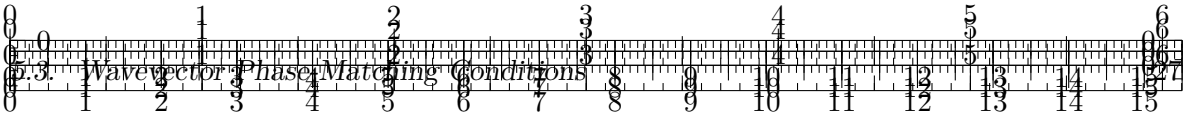

**Figure 5.1:** Comparison of experimental setups for (a) phase-matching-based signal detection using non-collinear beam geometry and (b) phase cycling-based signal isolation using collinear geometry. Phase cycling allows for simpler experimental setups at the cost of requiring multiple measurements with varied pulse phases.

- It allows for simpler optical setups with collinear or partially collinear beam geometries
- It enables effective background suppression, particularly of scatter and lower-order contributions
- It facilitates the separation of rephasing and nonrephasing pathways within the same measurement series
- It can be implemented in experimental setups where traditional phase-matching is challenging, such as in multidimensional infrared spectroscopy

In modern multidimensional spectroscopy, phase cycling is often combined with phase matching to achieve optimal signal isolation and background suppression [18, 43].

### 5.3.5 Phase-Cycling Fourier Selection and Construction of Absorptive 2D Spectra

The phase-cycling procedure provides an algebraic alternative (or complement) to spatial phase-matching (cf. Eqs. (5.15), (5.17)) for isolating specific third-order Liouville pathways in four-wave mixing experiments [7, 10, 14, 20, 30].
The nonlinear polarization induced by three incident pulses can be expressed as a Fourier series in the pulse phases $\phi_1, \phi_2, \phi_3$, and individual phase-matched components are isolated via an inverse Fourier transform:

$$P_{n_1,n_2,n_3}(t_{\mathrm{coh}}, T, t_{\mathrm{det}}) = \frac{1}{(2\pi)^3} \int_0^{2\pi} d\phi_1 \int_0^{2\pi} d\phi_2 \int_0^{2\pi} d\phi_3 \; e^{-i(n_1\phi_1 + n_2\phi_2 + n_3\phi_3)} P(\phi_1, \phi_2, \phi_3; t_{\mathrm{coh}}, T, t_{\mathrm{det}}). \tag{5.18}$$

The physically relevant phase-matching directions correspond to:

$$\vec{k}_{\mathrm{R}} = -\vec{k}_1 + \vec{k}_2 + \vec{k}_3, \qquad (n_1, n_2, n_3) = (-1, +1, +1), \tag{5.19}$$

$$\vec{k}_{\mathrm{NR}} = +\vec{k}_1 - \vec{k}_2 + \vec{k}_3, \qquad (n_1, n_2, n_3) = (+1, -1, +1), \tag{5.20}$$

yielding the rephasing (R) and nonrephasing (NR) contributions, respectively.
The emitted field in a given phase-matching direction is proportional to the corresponding polarization:

$$E_{k_s}(t_{\mathrm{coh}}, T, t_{\mathrm{det}}) \propto i P_{\vec{k}_S}(t_{\mathrm{coh}}, T, t_{\mathrm{det}}). \tag{5.21}$$

The nonlinear polarization is measured (or computed) on a discrete three-dimensional grid of controlled carrier-envelope phases for this FWM experiment with three pulses:

$$P(\phi_1, \phi_2, \phi_3; t_{\mathrm{coh}}, T, t_{\mathrm{det}}), \qquad \phi_1 = \frac{2\pi m}{M}, \; m = 0, \ldots, M-1, \tag{5.22}$$

with $M$ phase steps per pulse. A discrete triple Fourier transform over the phases yields the phase-resolved polarization components:

$$P_{n_1 n_2 n_3}(t_{\mathrm{coh}}, T, t) = \frac{1}{M^3} \sum_{a,b,c=0}^{M-1} P(\phi_1, \phi_2, \phi_3; t_{\mathrm{coh}}, T, t_{\mathrm{det}})\, e^{-i(n_1\phi_1 + n_2\phi_2 + n_3\phi_3)}. \tag{5.23}$$

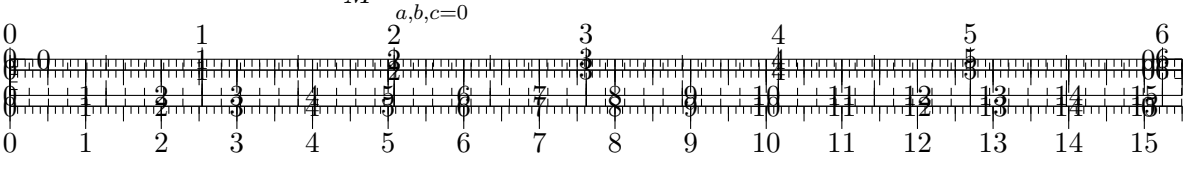

The (wavevector) phase-matched rephasing signal direction $\vec{k}_R = -\vec{k}_1 + \vec{k}_2 + \vec{k}_3$ (Eq. (5.16)) corresponds to selecting the Fourier index triple $(n_1, n_2, n_3) = (-1, +1, +1)$, while the nonrephasing direction $\vec{k}_{NR} = +\vec{k}_1 - \vec{k}_2 + \vec{k}_3$ corresponds to $(+1, -1, +1)$ [10, 14, 30]. The electric field that is radiated by the sample is proportional to the polarization

$$E_{k_s}(t_{\mathrm{coh}}, T, t_{\mathrm{det}}) \propto iP_{-1,+1,+1}(t_{\mathrm{coh}}, T, t_{\mathrm{det}}). \tag{5.24}$$

This reflects propagation factors and (typically weak) frequency-dependent constants relating polarization to the emitted heterodyne-detected field [14, 30].

**Time–Frequency Transforms.** After phase selection, the complex time-domain fields $E_R(t_{\mathrm{coh}}, T, t_{\mathrm{det}})$ and $E_{NR}(t_{\mathrm{coh}}, T, t_{\mathrm{det}})$ are Fourier transformed over the detection time $t_{\mathrm{det}}$ and the coherence time $t_{\mathrm{coh}}$ to construct the two-dimensional spectra (cf. Eq. (5.28)):

$$S_R(\omega_{\mathrm{coh}}, T, \omega_{\mathrm{det}}) = \int dt_{\mathrm{coh}} \int dt_{\mathrm{det}}\; e^{+i\omega_{\mathrm{coh}} t_{\mathrm{coh}}} e^{-i\omega_{\mathrm{det}} t_{\mathrm{det}}} E_R(t_{\mathrm{coh}}, T, t_{\mathrm{det}}), \tag{5.25}$$

$$S_{NR}(\omega_{\mathrm{coh}}, T, \omega_{\mathrm{det}}) = \int dt_{\mathrm{coh}} \int dt_{\mathrm{det}}\; e^{-i\omega_{\mathrm{coh}} t_{\mathrm{coh}}} e^{-i\omega_{\mathrm{det}} t_{\mathrm{det}}} E_{NR}(t_{\mathrm{coh}}, T, t_{\mathrm{det}}), \tag{5.26}$$

The opposite sign in the $t_{\mathrm{coh}}$-exponent implements the standard convention distinguishing rephasing (photon-echo) and nonrephasing contributions [10, 14]. In discrete numerical implementations, Eqs. (5.25)–(5.26) are approximated by (shifted) fast Fourier transforms; care must be taken to (i) include the sampling factors, (ii) verify axis centering ($\omega = 0$), and (iii) implement the $+i\omega_{\mathrm{coh}} t_{\mathrm{coh}}$ kernel for the rephasing branch (e.g. via complex conjugation tricks or inverse transforms) [10, 14].

**Global Phase and Absorptive Combination.** The experimentally measured (or simulated) complex spectra $S_R$ and $S_{NR}$ each carry unknown global phases (e.g. local oscillator offset). A relative phase $\varphi_g$ must be determined before constructing the absorptive (purely in-phase) 2D spectrum [14, 20, 30]. A common strategy is to optimize $\varphi_g$ so that the projection onto the detection axis reproduces an independently measured linear (or pump–probe) absorption spectrum or minimizes dispersive (derivative-like) features in selected slices:

$$S_{\mathrm{abs}}(\omega_{\mathrm{coh}}, T, \omega_{\mathrm{det}}) = \Re\left\{ S_R(\omega_{\mathrm{coh}}, T, \omega_{\mathrm{det}}) + e^{i\varphi_g} S_{NR}(\omega_{\mathrm{coh}}, T, \omega_{\mathrm{det}}) \right\}. \tag{5.27}$$

When phase referencing is stable (e.g. interferometric phase stabilization), $\varphi_g$ may be close to zero but still requires verification [7, 14]. The absorptive spectra is free from broadening refractive contributions [13].

**Normalization and Practical Considerations.** (i) The $M^{-3}$ factor in Eq. (5.23) should be retained (or absorbed consistently) for quantitative comparisons. (ii); omission rescales amplitudes and can obscure quantitative lineshape analysis [10, 14]. (iii) Frequency axes must be aligned so that $\omega_{\mathrm{coh}}$ for $S_R$ and $S_{NR}$ are defined with the same orientation before Eq. (5.27) is applied. (iv) Consistent sign conventions are essential; mixing conventions leads to mirrored or dispersive residual features [10, 14, 30].

**Summary.** Phase-cycling Fourier selection (Eqs. (5.18), (5.23)) cleanly isolates rephasing and nonrephasing field components (Eqs. (5.19)–(5.20)) without relying solely on spatial separation. The emitted fields are proportional to the corresponding polarizations (Eq. (5.21)). Subsequent bidimensional Fourier transforms with pathway-specific phase kernels (Eqs. (5.25)–(5.26)) and careful global phasing yield the absorptive 2D spectrum (Eq. (5.27)), which most directly reflects underlying transition energies, homogeneous/inhomogeneous broadening, and coherent couplings [10, 14, 30].

## 5.4 Photon Echo Spectroscopy

Photon echo spectroscopy is a powerful nonlinear optical technique used to eliminate inhomogeneous broadening and probe dynamic processes in complex systems [19, 30]. It represents a time-domain analog of spectral hole-burning.

### 5.4.1 Principle of Photon Echo

The photon echo phenomenon arises from the rephasing of coherences in an ensemble of quantum systems. In the simplest case of a two-pulse photon echo:

1. The first pulse creates a coherent superposition between ground and excited states.
2. During a waiting period $t_{\text{coh}}$, the coherences evolve at different frequencies due to inhomogeneous broadening, resulting in phase dispersion.
3. The second pulse, applied at time $t_{\text{coh}}$ after the first, effectively reverses the phase evolution of the coherences.
4. At time $2t_{\text{coh}}$, the phases realign (rephase), producing a macroscopic polarization that emits an echo signal.

The photon echo signal is the time-domain manifestation of that same rephasing process: when the system rephases, the third-order polarization emits a coherent burst of light (the photon echo) in that same phase-matching direction. This coherent emission occurs precisely when the individual molecular coherences realign in phase, creating a macroscopic polarization that radiates the echo signal.
The echo intensity as a function of the delay time $t_{\text{coh}}$ reveals information about the dephasing processes in the system.
It is important to emphasize that static inhomogeneity is crucial for the appearance of the photon echo signal. This inhomogeneity arises from variations in the local environment of individual quantum systems within the ensemble, leading to a distribution of transition frequencies. In numerical simulations and theoretical treatments, static inhomogeneity is taken into account by averaging the results over an ensemble of different realizations of the Hamiltonian [10, 30]. Without this inhomogeneous distribution, all systems would evolve identically, and the characteristic echo phenomenon would not occur.

### 5.4.2 Three-Pulse Photon Echo

The three-pulse photon echo extends the basic two-pulse technique by introducing a population period. The pulse sequence is as follows:

1. The first pulse creates coherences.
2. After time $t_{\text{coh}}$, the second pulse converts these coherences to populations.
3. During a waiting time $T$, population relaxation and spectral diffusion can occur.
4. The third pulse, applied at time $T$ after the second, reconverts populations to coherences.
5. At time $t_{\text{coh}}$ after the third pulse, the echo signal is emitted.

By scanning the waiting time $T$, this technique allows measurement of population dynamics and spectral diffusion processes.

### 5.4.3 Two-Dimensional Electronic Spectroscopy

Two-dimensional electronic spectroscopy (2DES) represents the state-of-the-art in photon echo techniques [7, 20, 38]. It correlates excitation and detection frequencies, revealing couplings between different transitions and energy transfer pathways.
In 2DES, the delay time $t_{\text{coh}}$ between the first and second pulses is systematically varied, and the signal field is detected in a phase-resolved manner using spectral interferometry

**REFERENCE:** find ref

Fourier transformation with respect to $t_{\text{coh}}$ yields the excitation frequency axis ($\omega_{\text{coh}}$), while spectral resolution of the signal provides the detection frequency axis ($\omega_t$).
The resulting 2D spectrum contains peaks along the diagonal ($\omega_{\text{coh}} = \omega_{\text{det}}$) corresponding to the linear absorption spectrum, while off-diagonal peaks reveal couplings and energy transfer between different states. The evolution of the 2D spectra with waiting time $T$ provides detailed information about energy transfer kinetics, spectral diffusion, and quantum coherence effects.
In experimental implementations, 2D spectra are often presented as the absorptive spectrum, which is given by the sum of the rephasing photon echo and nonrephasing spectra [10]. This representation eliminates phase-twist lineshapes and yields purely absorptive features that most directly correlate with the underlying energy level structure and couplings.

$$S(\omega_{\text{coh}}, T, \omega_{\text{det}}) = \iint dt_{\text{det}}\, dt_{\text{coh}}\, e^{i\omega_{\text{det}} t_{\text{det}}} e^{-i\omega_{\text{coh}} t_{\text{coh}}} S(t_{\text{coh}}, T, t_{\text{det}}) \tag{5.28}$$

where $S(t_{\text{coh}}, T, t_{\text{det}})$ is the time-domain signal.

### 5.4.4 Heterodyne and Homodyne Detection

The detection scheme plays a crucial role in nonlinear spectroscopy, affecting both the sensitivity and the information content of the measurements. Two primary detection methods are employed in multidimensional spectroscopy: homodyne and heterodyne detection

**REFERENCE:** find ref

#### Homodyne Detection

In homodyne detection, the intensity of the emitted signal field is measured directly:

$$S_{\text{homodyne}} \propto |E_{\text{sig}}|^2 \propto |P^{(3)}|^2 \tag{5.29}$$

where $E_{\text{sig}}$ is the signal electric field and $P^{(3)}$ is the third-order polarization. While experimentally simpler, homodyne detection has several limitations:

- It measures only the signal intensity, losing phase information
- The signal scales as the square of the third-order response
- Background-free detection requires careful phase-matching
- It is more susceptible to noise at low signal levels

#### Heterodyne Detection

Heterodyne detection involves the interference of the signal field with a reference field (local oscillator, LO) of known amplitude and phase:

$$S_{\text{heterodyne}} \propto |E_{\text{sig}} + E_{\text{LO}}|^2 \approx |E_{\text{LO}}|^2 + 2|E_{\text{LO}}||E_{\text{sig}}| \cos(\phi_{\text{LO}} - \phi_{\text{sig}}) + |E_{\text{sig}}|^2 \tag{5.30}$$

Since $|E_{\text{LO}}| \gg |E_{\text{sig}}|$, the cross-term dominates, and the signal can be extracted by phase-cycling or lock-in detection. Heterodyne detection offers several advantages

**REFERENCE:** find ref

- It provides both amplitude and phase information of the signal
- The signal scales linearly with the third-order response
- It offers enhanced sensitivity through amplification by the local oscillator
- It allows for a more direct connection to theoretical models

In modern multidimensional spectroscopy, spectral interferometry—a form of heterodyne detection—is widely employed [19]. The signal field and a time-delayed reference pulse are spatially overlapped and spectrally resolved using a spectrometer. The resulting interferogram in the frequency domain contains the complete information about the signal field's amplitude and phase.

### 5.4.5 Applications of Photon Echo Spectroscopy

Photon echo techniques have been applied to a wide range of problems across chemistry, biology, and materials science:

- **Exciton dynamics** in photosynthetic complexes, revealing quantum coherent energy transfer pathways

  **REFERENCE:** find ref

- **Vibrational dynamics** in proteins and liquids, elucidating structural fluctuations and hydrogen-bonding networks [17]
- **Charge transfer processes** in organic photovoltaics and light-harvesting systems
- **Coupling mechanisms** between electronic and vibrational degrees of freedom [22]

The ability of these techniques to separate homogeneous and inhomogeneous broadening, while providing time-resolved information about energy transfer and dephasing processes, makes them indispensable tools in modern physical chemistry and biophysics.

## 5.5 Advanced Spectroscopic Methods

Building upon the principles discussed in previous sections, several advanced spectroscopic techniques have been developed to address specific scientific questions. These methods combine the principles of nonlinear optics, phase-matching, and coherence phenomena to provide unprecedented insights into complex systems.

### 5.5.1 Multidimensional Infrared Spectroscopy

Similar to 2DES, two-dimensional infrared (2DIR) spectroscopy correlates vibrational transitions, providing information about molecular structure, conformational dynamics, and vibrational coupling [17, 22]. The technique is particularly powerful for studying hydrogen bonding networks, protein secondary structure, and chemical reaction dynamics.
In 2DIR, cross-peaks between different vibrational modes reveal anharmonic coupling and energy transfer pathways, while the lineshapes encode information about structural heterogeneity and dynamics [22]. Time-resolved 2DIR further allows tracking of structural changes during chemical reactions or conformational transitions [11].

### 5.5.2 Coherent Raman Techniques

Coherent anti-Stokes Raman scattering (CARS) and stimulated Raman scattering (SRS) are nonlinear optical techniques that provide enhanced sensitivity compared to spontaneous Raman spectroscopy [5]. These methods are widely used for chemically-specific microscopy without fluorescent labels.
In CARS, three fields with frequencies $\omega_1$, $\omega_2$, and $\omega_3$ generate a signal at frequency $\omega_s = \omega_1 - \omega_2 + \omega_3$ when the frequency difference $\omega_1 - \omega_2$ matches a vibrational resonance. The coherent nature of the process leads to signal enhancement compared to spontaneous Raman scattering.

### 5.5.3 Transient Absorption Spectroscopy

Transient absorption spectroscopy, also known as pump-probe spectroscopy, is a powerful technique for studying excited-state dynamics

**REFERENCE:** find ref

In this method, a short pump pulse excites the sample, and a subsequent probe pulse measures the resulting changes in absorption as a function of the time delay between the pulses.
The transient absorption signal $\Delta A$ can be expressed as:

$$\Delta A(t, \lambda) = -\log\left(\frac{I_{\text{pump-on}}(t, \lambda)}{I_{\text{pump-off}}(\lambda)}\right) \tag{5.31}$$

where $I_{\text{pump-on}}$ and $I_{\text{pump-off}}$ represent the transmitted probe intensity with and without the pump pulse, respectively.
Features in transient absorption spectra include ground-state bleaching, stimulated emission, excited-state absorption, and product absorption. Each of these contributions reflects different physical processes

**REFERENCE:** find ref

- **Ground-State Bleaching (GSB):** The pump pulse depletes the ground state population, resulting in decreased absorption of the probe pulse from the ground state. This appears as a negative signal in transient absorption spectra, coinciding spectrally with the ground-state absorption.
- **Stimulated Emission (SE):** When the probe pulse interacts with molecules in the excited state, it can stimulate emission back to the ground state. This process also yields a negative signal, typically red-shifted relative to the GSB due to the Stokes shift.

- **Excited-State Absorption (ESA):** Molecules in the excited state can absorb the probe pulse, transitioning to even higher excited states. This process yields a positive signal in the transient absorption spectrum, as it represents additional absorption that occurs only when the sample is excited.

Figure **??** illustrates these three primary contributions to transient absorption signals.
Analysis of these features as a function of time delay provides information about excited-state lifetimes, energy transfer processes, and photochemical reaction pathways. The ability to separate and identify these contributions is crucial for understanding the dynamics of complex molecular systems

**REFERENCE:** find ref

## 5.6 Multidimensional Spectroscopy in Structural Biology and Chemistry

### 5.6.1 Time- and Structure-Resolution Challenges

Scientific questions encompassing both the structure and dynamics of molecular systems present significant experimental challenges [17]. Consider fundamental processes such as protein folding, solvent fluctuations, or electron transfer reactions. In each case, researchers seek to understand the reaction pathway, which requires time-resolving the molecular structure. However, the relevant time scales can span an enormous range—from femtoseconds to hours—depending on the specific system under investigation.
Traditional spectroscopic methods face inherent limitations in simultaneously achieving high temporal and structural resolution. When dynamics occur on slow time scales, nuclear magnetic resonance (NMR) spectroscopy can provide exquisite structural information with atomic-level detail. Conversely, for fast processes, fluorescence or absorption spectroscopy can probe dynamics with exceptional temporal resolution, but with a corresponding trade-off in structural specificity [17]. Between these extremes lies an experimental gap in both time- and structure-resolution capabilities.
This gap becomes even more pronounced when studying dynamics in confined environments such as biological membranes, where many standard structural techniques become difficult or impossible to apply. The challenge is particularly acute for intermediate time scales (picoseconds to microseconds) and for systems where both structural changes and dynamic processes are coupled.

### 5.6.2 2D IR Spectroscopy: Bridging the Gap

Two-dimensional infrared (2D IR) spectroscopy has emerged as a powerful technique to address these limitations, providing bond-specific structural resolution across all relevant time scales [17]. This technique offers several unique advantages:

- **Temporal versatility:** 2D IR spectroscopy possesses the fast time resolution necessary to follow electron transfer and solvent dynamics on femtosecond time scales, while also being applicable in ”snapshot” mode to study kinetics extending to arbitrarily long time scales.

- **Sample flexibility:** The technique can be applied to diverse sample types, including dilute solutions, solid-state systems, and membrane-bound proteins, making it particularly valuable for biological applications.

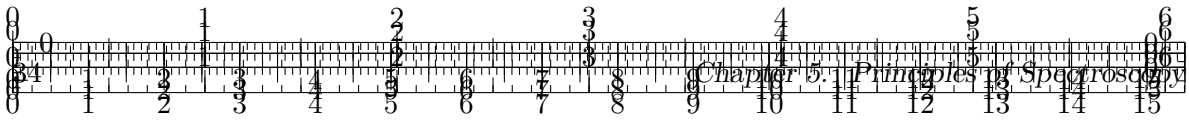


- **Structural sensitivity:** The method derives its structural information from couplings between vibrational modes that give rise to characteristic infrared bands and cross-peaks. These cross-peaks provide direct information about molecular connectivity and conformational changes.

- **Environmental probes:** Molecular structures can be probed through hydrogen bonding patterns and electric field effects that generate dynamic 2D lineshapes, providing insights into local environments and intermolecular interactions.

The structural sensitivity of 2D IR spectroscopy stems from the fact that vibrational frequencies are exquisitely sensitive to local molecular environment, hydrogen bonding, and electrostatic interactions. Cross-peaks in 2D IR spectra arise from vibrational coupling and provide direct information about spatial proximity and connectivity between different molecular groups [17].

### 5.6.3 Computational Integration and Future Directions

A particularly powerful aspect of 2D IR spectroscopy is that the spectra can be quantitively computed from molecular dynamics simulations, providing a direct comparison between experimental observations and all-atom theoretical models [17]. This computational-experimental synergy enables:

- Validation of molecular dynamics force fields and simulation protocols
- Assignment of spectral features to specific molecular structures and conformations
- Prediction of spectroscopic signatures for proposed molecular mechanisms
- Development of structure-spectrum relationships for complex systems

While 2D IR spectroscopy can be used qualitatively as an analytical tool, a deeper understanding of nonlinear optics, vibrational potentials, and lineshape theory enables much more sophisticated interpretation of 2D spectra and expands the range of possible applications [17]. The principles and methods developed for 2D IR spectroscopy also extend to 2D visible spectroscopy, which probes electronic transitions and has found particular application in studying photosynthetic light-harvesting complexes and other photobiological systems. Looking toward the future, pulse sequences for three-dimensional (and higher-dimensional) spectroscopy are being developed, promising even greater structural and dynamical information content [17].
The integration of multidimensional spectroscopic techniques with advanced computational methods represents a paradigm shift in how complex molecular systems can be studied, offering unprecedented insights into the relationship between molecular structure, dynamics, and function.

## 5.7 Summary and Outlook

Spectroscopy continues to evolve as a cornerstone analytical technique in physical sciences [10, 30]. From the basic principles of light-matter interaction to advanced nonlinear methods, spectroscopic approaches provide unique insights into the structure, dynamics, and function of complex systems across multiple time and length scales.
Recent developments in laser technology, detection methods, and theoretical frameworks have expanded the frontiers of spectroscopy [20]

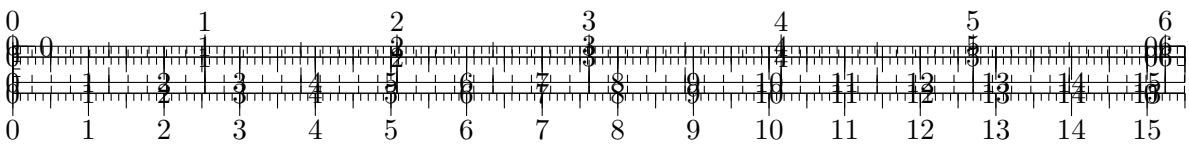

**REFERENCE:** find ref

Attosecond spectroscopy now probes electron dynamics on their natural time scale, while quantum light sources open new possibilities for quantum-enhanced measurements.
The integration of spectroscopic methods with imaging techniques, such as super-resolution microscopy and spectroscopic tomography, bridges the gap between molecular-level information and macroscopic observations [7]. Meanwhile, the application of artificial intelligence and machine learning approaches to spectral data analysis promises to reveal subtle patterns and correlations that might otherwise remain hidden.
As our understanding of light-matter interactions deepens and experimental capabilities advance, spectroscopy will continue to provide critical insights across chemistry, physics, biology, and materials science, contributing to technological innovations and fundamental scientific discoveries.

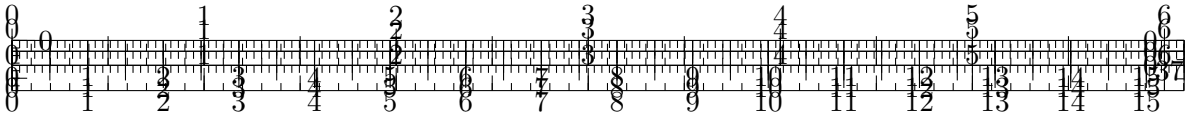

# Chapter 6

# Model Systems

Having developed the two-dimensional spectroscopic formalism and open-system dynamics earlier, we now transition to applying the photon-echo spectroscopy workflow to concrete models. We start from minimal reference systems (a single qubit and a four-level system formed by two coupled qubits) and then generalize to $N$ qubits arranged on a cylindrical geometry, mirroring the architectural motifs of microtubules where each site represents a bonding location in the molecular scaffold [21]. Throughout, we connect to standard third-order spectroscopy concepts [10, 20, 30] and use the master-equation tools introduced previously (see Chapter 2; cf. [6, 33]).

## 6.1 Reference Models

### 6.1.1 Qubit Model

Single two-level systems (spin–boson model) are the canonical testbed in open-quantum-system theory; their weak-coupling dynamics under Redfield and Lindblad-type generators are well characterized [6, 8, 28, 33], with standard choices of bath spectral densities (e.g., Ohmic or Drude–Lorentz) [34]. As a representative study, polarization-resolved dephasing and relaxation of a qubit coupled to a bosonic bath has been analyzed within Redfield theory in [31], providing a useful baseline against which to benchmark our spectroscopy workflow.

The qubit system Hamiltonian is given by $H_{\mathrm{S}} = \frac{\omega}{2}\sigma_z$, or equivalently

$$H_{\mathrm{S}} = \omega \left|e\right\rangle \left\langle e\right|, \tag{6.1}$$

where $\omega$ is the qubit transition frequency, $\sigma_z$ is the Pauli operator in z direction. The environment is characterized by a spectral density $J(\omega)$ (cf. [6, 34]). In the photon-echo context, the system-field interaction in the dipole approximation enters the third-order response, while the reduced dynamics may be propagated with the Redfield or Lindblad-type generators derived in Chapter 2 (see also [8, 28]).

For spectroscopy, we assume a system dipole operator $\hat{\mu}_{\mathrm{S}} = \mu\,\sigma_x$ (oriented relative to the laboratory frame by the polarization geometry), and compute the rephasing and nonrephasing third-order signals using the response-function formalism [20, 30].

**IDEA:** explain that this simplest two level system only offers limited insights, but is a good test case for the workflow. This is due to the lack of multiple states and pathways, which are essential for capturing the rich dynamics and interactions detectable with 2D spectroscopy.

### 6.1.2 4-Level System (Two Qubits)

Extending to two coupled qubits, we obtain a four-level manifold spanned by $\{\left|gg\right\rangle, \left|ge\right\rangle, \left|eg\right\rangle, \left|ee\right\rangle\}$. A convenient system Hamiltonian is

$$H_{\mathrm{S}}^{(2)} = \sum_{i=1}^{2} \frac{\omega_i}{2}\,\sigma_z^{(i)} + J\left(\sigma_+^{(1)}\sigma_-^{(2)} + \sigma_-^{(1)}\sigma_+^{(2)}\right), \tag{6.2}$$

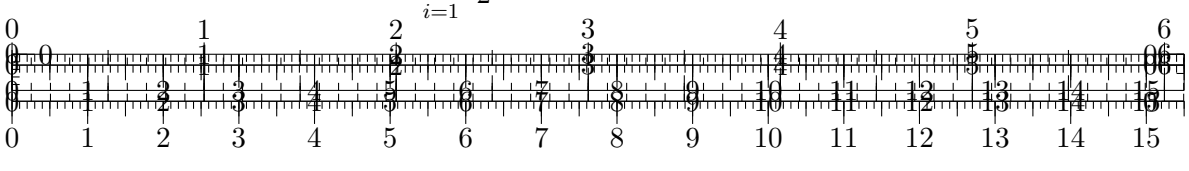

with coherent exchange coupling $J$. For open dynamics we consider independent local baths,

$$H_{\mathrm{B}}^{(2)} = \sum_{i=1}^{2} \sum_{k} \omega_{k,i}\, a_{k,i}^{\dagger} a_{k,i}, \quad H_{\mathrm{SB}}^{(2)} = \sum_{i=1}^{2} \sum_{k} g_{k,i} \left(\sigma_{+}^{(i)} a_{k,i} + \sigma_{-}^{(i)} a_{k,i}^{\dagger}\right), \tag{6.3}$$

though correlated baths can be accommodated as discussed in Chapter 2. This minimal dimer already exhibits cross-peaks and coherence transfer in photon-echo spectra [32], making it a natural benchmark for the workflow.

## 6.2 Generalization to $N$ Qubits on Cylindrical Geometry

Motivated by the protofilament arrangement in microtubules, we place $N$ qubits on a discretized cylindrical surface. The interaction energy of two such sites is given by isotropic dipole couplings of the form [15]

$$J_{ij} \propto \frac{1}{\|\vec{r}_{ij}\|^3} \left[\vec{\mu}_i \cdot \vec{\mu}_j - 3\,(\vec{\mu}_i \cdot \hat{\vec{r}}_{ij})(\vec{\mu}_j \cdot \hat{\vec{r}}_{ij})\right], \tag{6.4}$$

where $\vec{\mu}_i$ are transition dipoles and $\vec{r}_{ij}$ the displacement between sites $i$ and $j$ (cf. [25, 29]).

Let $N_\theta$ be the number of sites per ring and $N_z$ the number of rings (so $N = N_\theta N_z$). We index sites by $(m, n)$ with $m \in \{0, \ldots, N_\theta - 1\}$ (azimuthal) and $n \in \{0, \ldots, N_z - 1\}$ (axial). The system Hamiltonian reads

$$H_{\mathrm{S}}^{(N)} = \sum_{n=1}^{N} \omega_n \left|n\right\rangle \left\langle n\right| + \sum_{m<n}^{N} J_{mn} \big(\sigma_{+}^{(m)} \sigma_{-}^{(n)} + \mathrm{h.c.}\big) \tag{6.5}$$

$$+ \sum_{m<n}^{N} (\omega_m + \omega_n) \left|m,n\right\rangle \left\langle m,n\right| + \sum_{mnl}^{N} \big[\big(J_{ml} \left|ln\right\rangle \left\langle mn\right| + J_{nl} \left|lm\right\rangle \left\langle mn\right|\big) + \mathrm{h.c.}\big] \tag{6.6}$$

implementing periodic boundary conditions in the azimuthal direction.

The bath part may be modeled as independent local environments or structured/collective baths,

$$H_{\mathrm{B}}^{(N)} = \sum_{m,n} \sum_{k} \omega_{k,(m,n)} a_{k,(m,n)}^{\dagger} a_{k,(m,n)}, \quad H_{\mathrm{SB}}^{(N)} = \sum_{m,n} \sum_{k} g_{k,(m,n)} \left(\sigma_{+}^{(m,n)} a_{k,(m,n)} + \mathrm{h.c.}\right), \tag{6.7}$$

with spectral densities chosen to reflect protein or solvent environments [34, 37].

This geometry captures collective transport pathways and their photon-echo signatures, offering a route to connect microscopic couplings to observed energy migration along microtubules [21]. It also allows us to compare rephasing/nonrephasing features and waiting-time dynamics against the reference dimer, thereby isolating geometric versus environmental contributions [30, 39].

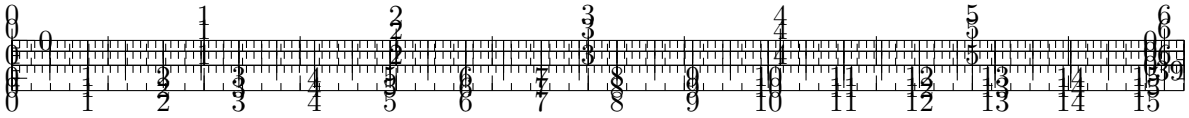

# Chapter 7

# Example of Todo Notes

## 7.1 Using Todo Notes

Here's an example paragraph with various todo notes embedded. The Fourier transform is a mathematical transform that decomposes a function into its constituent frequencies.

**IMPORTANT:** Complete this explanation with the formal definition!

When discussing the Hamiltonian of a quantum system, we typically write it as:

$$H = H_0 + H_{\text{int}} \tag{7.1}$$

**EQUATION:** Add the interaction terms explicitly

The spectroscopic signals in 2D spectroscopy contain peaks along the diagonal corresponding to the linear absorption spectrum.

**REFERENCE:** Add reference to Mukamel's work

In the phase-matching conditions section we could

**IDEA:** Add a diagram illustrating the k-vector directions in FWM experiments

The derivation of the optical Bloch equations needs

**FIX:** Fix the coherence evolution equation - sign error in the term involving $\rho_{21}$

## 7.2 Summary of Todo Types

- `todoimp{}` - Red notes for high importance items
- `todoidea{}` - Green notes for ideas and suggestions
- `todoeq{}` - Blue notes for equations and mathematical content
- `todoref{}` - Purple notes for references and citations
- `todofix{}` - Orange notes for text that needs correction

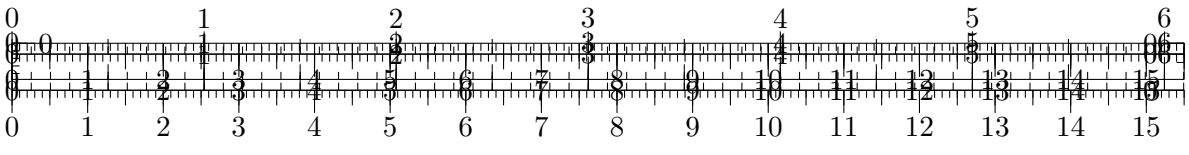

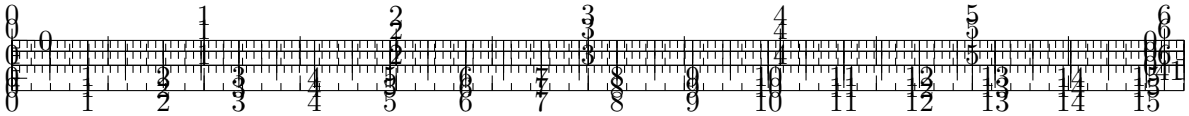

# Bibliography


[1] D. Abramavicius, B. Palmieri, D. V. Voronine, F. Sanda, and S. Mukamel, "Coherent multidimensional optical spectroscopy of excitons in molecular aggregates; quasiparticle versus supermolecule perspectives", en, Chem. Rev. **109**, 2350–2408 (2009).

[2] T. Albash, S. Boixo, D. A. Lidar, and P. Zanardi, "Quantum adiabatic Markovian master equations", en, New J. Phys. **14**, 123016 (2012).

[3] I. Bogacz, E. Szilagyi, H. Makita, P. S. Simon, M. Zhang, M. D. Doyle, K. Chatterjee, M. Kretzschmar, P. Chernev, N. Croy, M.-H. Cheah, M. Dasgupta, I. Nangca, T. Fransson, A. Bhowmick, A. S. Brewster, N. K. Sauter, S. Owada, K. Tono, S. Zerdane, A. Oggenfuss, D. Babich, M. Sander, R. Mankowsky, H. T. Lemke, L. B. Gee, T. Sato, T. Kroll, J. Messinger, R. Alonso-Mori, U. Bergmann, D. Sokaras, V. K. Yachandra, J. Kern, and J. Yano, "X-ray absorption spectroscopy of dilute metalloenzymes at X-ray free-electron lasers in a shot-by-shot mode", en, J. Phys. Chem. Lett. **16**, 3778–3787 (2025).

[4] R. W. Boyd, "Chapter 1 - the nonlinear optical susceptibility", en, in *Nonlinear Optics (third Edition)*, edited by R. W. Boyd (Academic Press, Burlington, Jan. 1, 2008), pp. 1–67.

[5] "Contents", en, in *Nonlinear Optics (third Edition)*, edited by R. W. Boyd, Third Edition (Academic Press, Burlington, 2008), pp. vii–xi.

[6] H.-P. Breuer and F. Petruccione, *The theory of open quantum systems*, en, 1. publ. in paperback, [Nachdr.] (Clarendon Press, Oxford, 2009), 613 pp.

[7] T. Brixner, T. Mančal, I. V. Stiopkin, and G. R. Fleming, "Phase-stabilized two-dimensional electronic spectroscopy", en, J. Chem. Phys. **121**, 4221–4236 (2004).

[8] F. Campaioli, J. H. Cole, and H. Hapuarachchi, "Quantum Master Equations: Tips and Tricks for Quantum Optics, Quantum Computing, and Beyond", en, PRX Quantum **5**, 020202 (2024).

[9] H. Carmichael, *An open systems approach to quantum optics: lectures presented at the université libre de bruxelles october 28 to November 4, 1991*, en, red. by H. Araki, E. Brézin, J. Ehlers, U. Frisch, K. Hepp, R. L. Jaffe, R. Kippenhahn, H. A. Weidenmüller, J. Wess, J. Zittartz, and W. Beiglböck, Vol. 18, Lecture Notes in Physics Monographs (Springer, Berlin, Heidelberg, 1993).

[10] M. Cho, *Two-dimensional optical spectroscopy*, en (CRC Press, Boca Raton, 2009), 378 pp.

[11] M. Fayer, "Dynamics of liquids, molecules, and proteins measured with ultrafast 2D IR vibrational echo chemical exchange spectroscopy", en, Annu. Rev. Phys. Chem. **60**, 21–38 (2009).

[12] R. Feynman, *The feynman lectures on physics vol. II ch. 11: inside dielectrics*, en, (1965) `https://www.feynmanlectures.caltech.edu/II_11.html` (visited on 07/04/2025).

[13] F. D. Fuller and J. P. Ogilvie, "Experimental implementations of two-dimensional fourier transform electronic spectroscopy", en, Annu. Rev. Phys. Chem. **66**, 667–690 (2015).


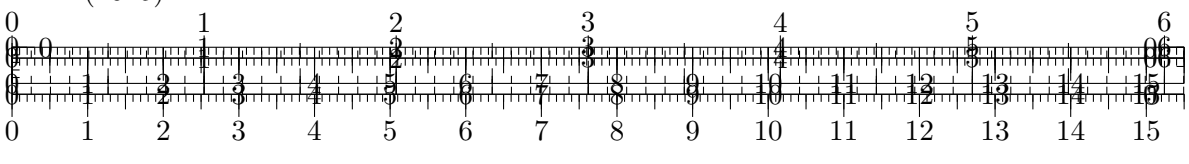

[14] D. Green, G. Bressan, I. A. Heisler, S. R. Meech, and G. A. Jones, "Vibrational coherences in half-broadband 2D electronic spectroscopy: spectral filtering to identify excited state displacements", en, J. Chem. Phys. **160**, 234104 (2024).

[15] D. J. Griffiths, *Introduction to electrodynamics*, en, 4. ed., international ed, Always Learning (Pearson, Boston, 2013), 599 pp.

[16] P. Hamm, "Principles of nonlinear optical spectroscopy: a practical approach", en, (2005).

[17] P. Hamm and M. Zanni, *Concepts and methods of 2D infrared spectroscopy*, en (Cambridge University Press, Cambridge, 2011).

[18] Z.-C. Huang-Fu, Y. Qian, T. Zhang, J. B. Brown, and Y. Rao, "Development of phase-cycling interface-specific two-dimensional electronic sum frequency generation (2D-ESFG) spectroscopy", The Journal of Chemical Physics **161**, 114201 (2024).

[19] J. D. Hybl, A. W. Albrecht, S. M. Gallagher Faeder, and D. M. Jonas, "Two-dimensional electronic spectroscopy", en, Chem. Phys. Lett. **297**, 307–313 (1998).

[20] D. M. Jonas, "Two-dimensional femtosecond spectroscopy", en, Annu. Rev. Phys. Chem. **54**, 425–463 (2003).

[21] A. P. Kalra, A. Benny, S. M. Travis, E. A. Zizzi, A. Morales-Sanchez, D. G. Oblinsky, T. J. A. Craddock, S. R. Hameroff, M. B. MacIver, J. A. Tuszyński, S. Petry, R. Penrose, and G. D. Scholes, "Electronic Energy Migration in Microtubules", en, ACS Cent. Sci. **9**, 352–361 (2023).

[22] M. Khalil, N. Demirdöven, and A. Tokmakoff, "Vibrational coherence transfer characterized with fourier-transform 2D IR spectroscopy", en, J. Chem. Phys. **121**, 362–373 (2004).

[23] T. D. Ladd, F. Jelezko, R. Laflamme, Y. Nakamura, C. Monroe, and J. L. O'Brien, "Quantum computers", en, Nature **464**, 45–53 (2010).

[24] N. Lambert, E. Giguère, P. Menczel, B. Li, P. Hopf, G. Suárez, M. Gali, J. Lishman, R. Gadhvi, R. Agarwal, A. Galicia, N. Shammah, P. Nation, J. R. Johansson, S. Ahmed, S. Cross, A. Pitchford, and F. Nori, *QuTiP 5: the quantum toolbox in python*, en, version 1, (Dec. 6, 2024) `http://arxiv.org/abs/2412.04705` (visited on 09/10/2025), pre-published.

[25] R. H. Lehmberg, "Radiation from an N -Atom System. I. General Formalism", en, Phys. Rev. A **2**, 883–888 (1970).

[26] L. Li, M. J. Hall, and H. M. Wiseman, "Concepts of quantum non-markovianity: a hierarchy", en, Phys. Rep. **759**, 1–51 (2018).

[27] G. Lindblad, "On the generators of quantum dynamical semigroups", en, Commun. Math. Phys. **48**, 119–130 (1976).

[28] D. Manzano, "A short introduction to the Lindblad master equation", AIP Adv. **10**, 025106 (2020).

[29] B. Masters, "Paths to Förster's resonance energy transfer (FRET) theory", en, Eur. Phys. J. H **39**, 87–139 (2014).

[30] S. Mukamel, *Principles of Nonlinear Optical Spectroscopy* (Oxford University Press, New York, 1995), 543 pp.

[31] T. Palm and P. Nalbach, "Dephasing and relaxational polarized sub-ohmic baths acting on a two-level system", en, J. Chem. Phys. **150**, 234108 (2019).

[32] A. V. Pisliakov, T. Mančal, and G. R. Fleming, "Two-dimensional optical three-pulse photon echo spectroscopy. II. Signatures of coherent electronic motion and exciton population transfer in dimer two-dimensional spectra", en, J. Chem. Phys. **124**, 234505 (2006).

[33] A. Redfield, "The theory of relaxation processes", en, in *Advances in Magnetic and Optical Resonance*, Vol. 1 (Elsevier, 1965), pp. 1–32.

[34] G. Ritschel and A. Eisfeld, "Analytic representations of bath correlation functions for ohmic and superohmic spectral densities using simple poles", en, J. Chem. Phys. **141**, 94101 (2014).

[35] Á. Rivas, S. F. Huelga, and M. B. Plenio, "Quantum non-markovianity: characterization, quantification and detection", en, version 2, `10.48550/ARXIV.1405.0303` (2014).

[36] Á. Rivas, A. D. K Plato, S. F. Huelga, and M. B Plenio, "Markovian master equations: a critical study", New Journal of Physics **12**, 113032 (2010).

[37] J. Roden, W. T. Strunz, K. B. Whaley, and A. Eisfeld, "Accounting for intra-molecular vibrational modes in open quantum system description of molecular systems", en, J. Chem. Phys. **137**, 204110 (2012).

[38] G. S. Schlau-Cohen, A. Ishizaki, and G. R. Fleming, "Two-dimensional electronic spectroscopy and photosynthesis: fundamentals and applications to photosynthetic light-harvesting", en, Chem. Phys. **386**, 1–22 (2011).

[39] J. Segarra-Martí, S. Mukamel, M. Garavelli, A. Nenov, and I. Rivalta, "Towards Accurate Simulation of Two-Dimensional Electronic Spectroscopy", Topics in Current Chemistry **376**, 24 (2018).

[40] H. Sun, U. Harbola, S. Mukamel, and M. Galperin, *Two-dimensional spectroscopy of open quantum systems*, (Dec. 14, 2024) `http://arxiv.org/abs/2412.10931` (visited on 02/11/2025), pre-published.

[41] Y. Tanimura, "Numerically "exact" approach to open quantum dynamics: the hierarchical equations of motion (HEOM)", en, J. Chem. Phys. **153**, 20901 (2020).

[42] Y. Tanimura and S. Mukamel, "Two-dimensional femtosecond vibrational spectroscopy of liquids", en, J. Chem. Phys. **99**, 9496–9511 (1993).

[43] P. Tian, D. Keusters, Y. Suzaki, and W. S. Warren, "Femtosecond phase-coherent two-dimensional spectroscopy", en, Science **300**, 1553–1555 (2003).

[44] N. Vogt, J. Jeske, and J. H. Cole, "Stochastic bloch-redfield theory: quantum jumps in a solid-state environment", en, Phys. Rev. B **88**, 174514 (2013).

[45] U. Weiss, *Quantum dissipative systems*, en, 4th ed. (WORLD SCIENTIFIC, Mar. 2012).